UNIVERSIDADE D
COIMBRA

Micael Frias Borges

EFEITO DAS PROPRIEDADES ELASTO-PLÁSTICAS NA PROPAGAÇÃO DE FENDAS POR FADIGA

Dissertação no âmbito do Mestrado Integrado em Engenharia Mecânica, na especialidade de Produção e Projeto orientada pelo Professor Doutor Fernando Jorge Ventura Antunes e pelo Professor Doutor Pedro André Dias Prates e apresentada ao Departamento de Engenharia Mecânica da Faculdade de Ciências e Tecnologia da Universidade de Coimbra.

Julho de 2019

1 2 9 0

FACULDADE DE CIÊNCIAS E TECNOLOGIA
UNIVERSIDADE D COIMBRA

Effect of elasto-plastic properties on fatigue crack growth

Submitted in Partial Fulfilment of the Requirements for the Degree of Master in Mechanical Engineering in the speciality of Production and Project

Efeito das propriedades elasto-plásticas na propagação de fendas por fadiga

Author

Micael Frias Borges

Advisors

Professor Doutor Fernando Jorge Ventura Antunes

Professor Doutor Pedro André Dias Prates

Jury

President	**Professor Doutor Diogo Mariano Simões Neto** **Professor Auxiliar da Universidade de Coimbra**
Vowels	**Professor Doutor Francisco Diaz Garrido** **Professor Titular da Universidade de Jaén** **Professor Doutor Ricardo Nuno Madeira Soares Branco** **Professor Auxiliar da Universidade de Coimbra**
Advisor	**Professor Doutor Fernando Jorge Ventura Antunes** **Professor Auxiliar da Universidade de Coimbra**

Coimbra, July, 2019

To my grandfather José Frias.

Strive for perfection in everything.

Take the best that exists and make it better.

If it doesn't exist, create it.

Accept nothing nearly right or good enough.

Sir Henry Royce

co-founder of Rolls Royce

ACKNOWLEDGEMENTS

First, I would like to express my deepest gratitude to my scientific advisor, Professor Fernando Antunes for the patience, encouragement, availability, guidance and valuable insights during this semester.

To my co-advisor Pedro Prates for his insights regarding the modelling of the elasto-plastic behaviour and strain hardening.

To Professor Marta Oliveira for the availability of the template and also for programming the non-contact simulations in DD3IMP.

To the Technology Group of the Mechanical Engineering Department for the availability of the finite element program DD3IMP.

To my parents, grandparents and sister for their support and encouragement through this hard and long journey. This step that now ends is not only for my effort but also yours.

Finally, a special thanks to my grandfather José Frias who, I am sure, will always be by my side.

This work was carried out under the project with reference: PTDC/CTM-CTM/29101/2017 – POCI-01-0145-FEDER-029101 sponsored by Fundo Europeu de Desenvolvimento Regional (FEDER), through the program COMPETE2020 - Programa Operacional Competitividade e Internacionalização (POCI) and with the financial support of FCT/MCTES through national funds (PIDDAC).

Abstract

Components submitted to cyclic loadings are liable to fail in service due to fatigue phenomenon. Predicting the service life of these components is essential, however, fatigue crack growth (FCG) is usually studied using da/dN -ΔK curves. Being FCG linked to irreversible phenomena happening at the crack tip and being the stress intensity factor, ΔK, an elastic parameter does not seem logic to apply this methodology. As such, in this work, ΔK is replaced by the plastic CTOD, a non-linear parameter.

In this thesis, a parametric study is performed relating the elasto-plastic properties with the plastic CTOD. The parameters studied were Young´s modulus (E), yield stress (Y_0), isotropic saturation stress (Y_{Sat}), Voce isotropic hardening parameter (C_Y), kinematic saturation stress (X_{Sat}) and Armstrong-Frederick hardening parameter (C_X), for two base materials: the 7050-T6 aluminium alloy and the 304L stainless steel. The main objectives of this work are therefore to study the effect of each property on plastic CTOD and compare the relationships with models found in the literature, which relates da/dN with material properties.

The elasto-plastic properties were changed in numerical simulations, assuming values of more and less 50% and 25% of the reference values. The simulations were performed with and without contact at the crack flanks, maintaining the specimen´s geometry, loading conditions and the stress state of the materials.

FCG rate was found to increase linearly with $1/E$ and $1/Y_0$, which is according to most of the models present in the literature. Some non-linearities were found in these relationships in simulations with crack closure. Y_{Sat}, X_{Sat}, C_X and C_Y were found to decrease non-linearly the FCG rate when these properties were increased. The Young´s modulus has relatively high sensitivity in δ_p and therefore its influence cannot be neglected. The yield stress was found to be the most sensitive parameter in SS304L, in simulations with contact, and AA7050-T6, in simulations without contact and the least sensitive in SS304L, in simulations without contact, and AA7050-T6, in simulations with contact. For the cases where the sensitivity of Y_0 decreased, the sensitivities of the saturation stresses increased, and vice-versa.

Keywords Fatigue crack growth, plastic CTOD, Young´s modulus, yield stress, crack closure, strain hardening.

Resumo

Componentes submetidos a cargas cíclicas podem falhar em serviço devido ao fenómeno de fadiga. Prever a vida útil destes componentes é essencial, no entanto, a propagação de fendas por fadiga (PFF) é habitualmente estudada usando curvas da/dN-ΔK. Estando a PFF ligada a fenómenos irreversíveis que ocorrem na extremidade da fenda e sendo o fator de intensidade de tensão, ΔK, um parâmetro elástico não parece lógico aplicar essa metodologia. Como tal, neste trabalho, ΔK é substituído pelo CTOD plástico, um parâmetro não linear.

Nesta tese, é realizado um estudo paramétrico para as propriedades elasto-plásticas, mais específicamente para o módulo de Young (E), tensão de cedência (Y_0), tensão de saturação isotrópica (YSat), parâmetro de encruamento isotrópico de Voce (C_Y), tensão de saturação cinemática (XSat) e parâmetro de encruamento de Armstrong-Frederick (C_X), para dois materiais de base: a liga de alumínio 7050-T6 e o aço inoxidável 304L. Os principais objetivos deste trabalho são pois: estudar o efeito de cada propriedade sobre o CTOD plástico e comparar as relações com modelos encontrados na literatura que relacionam da/dN com propriedades do material. As propriedades elasto-plásticas foram alteradas em simulações numéricas, assumindo valores de mais e menos 50% e 25% dos valores de referência. As simulações são realizadas com e sem contacto nos flancos das fendas, mantendo a geometria do provete, as condições de carregamento e estado de tensão dos materiais.

Verificou-se que a taxa de PFF aumenta linearmente com $1/E$ e $1/Y_0$, o que está de acordo com a maioria dos modelos presentes na literatura. Algumas não-linearidades são encontradas nessas relações em simulações com fecho de fenda. YSat, X_{Sat}, C_X e C_Y diminuíram não linearmente a PFF quando estas propriedades foram aumentadas. O módulo de Young tem sensibilidade relativamente alta em δ_p e, portanto, a influência desse parâmetro não pode ser desprezada. A tensão de cedência foi encontrada como o parâmetro mais sensível no aço inoxidável 304L, em simulações com contacto, e na liga de alumínio 7050-T6, em simulações sem contacto e as menos sensíveis no aço inoxidável 304L, em simulações sem contacto, e liga de alumínio 7050-T6, em simulações

com contacto. Para os casos em que a sensibilidade de Y_0 diminuiu, as sensibilidades das tensões de saturação aumentaram e vice-versa.

Palavras-chave: Propagação de fendas por fadiga, CTOD plástico, módulo de Young, tensão de cedência, fecho de fenda, encruamento por deformação.

Contents

LIST OF FIGURES

LIST OF TABLES

LIST OF SYMBOLS AND ACRONYMS

List of Symbols

$\boldsymbol{A}$ – set of Voce and Armstrong & Frederick parameters that minimises $F(\mathbf{A})$

a – Crack length

a_0 – Initial crack length

b, p – Constants of the polynomial relationship between da/dN and $\Delta CTOD_p$

C, m – Constants of the Paris Erdogan law obtained experimentally

c – Constant

C_X – Parameter of the Armstrong & Frederick kinematic law

C_Y – Parameter of the Voce isotropic law

da/dN – Fatigue crack growth rate

E – Young´s modulus

$\mathcal{F}$ – Function defining the yielding condition

F – Applied load

$F(\boldsymbol{A})$ – Cost function

F_{open} – Crack opening load

F_{max} – Maximum load in a loading cycle

F_{min} – Minimum load in a loading cycle

K – Stress intensity factor

$K_{1C}(K_C)$ – Fracture toughness

K_{max} – Maximum stress intensity factor

K_{min} – Minimum stress intensity factor

K_{open} – K value where the crack opens

$U_{closure}$ – Portion of load cycle during which the crack is closed

R – Stress ratio

r_{pc} – Radius of inverse plastic zone

$\boldsymbol{X}$ – Deviatoric back-stress tensor

X_{Sat} – Kinematic saturation stress

Y – Geometric parameter

Y_0 – Yield stress

Y_{Sat} – Isotropic saturation stress

δ_e – Elastic CTOD range

δ_p – Plastic CTOD range

Δa – Crack advance

ΔK– Stress intensity factor range

ΔK_{eff}– Effective stress intensity factor range

ΔK_{th}– Fatigue threshold

$\Delta \varepsilon_{p,yy}$– Plastic deformation range along y direction

$\bar{\varepsilon}^p$– Equivalent plastic strain

$\dot{\bar{\varepsilon}}^p$– Equivalent plastic strain rate

$\sigma^{Exp}(\boldsymbol{A})$ – Experimentally measured values of true stress

$\sigma^{Fit}(\boldsymbol{A})$ – Fitted measured values of true stress

$\boldsymbol{\sigma'}$ – Deviatoric Cauchy stress tensor

$\bar{\sigma}$– Equivalent stress tensor

σ– Nominal stress

σ_{max} – Maximum stress

σ_{min} – Minimum stress

σ_{ys} – Yield stress (chapter 2)

σ_0 – Yield stress (chapter3)

ν– Poisson´s coefficient

∇f– Sensitivity coefficient

λ – Constant

Acronyms

3D – Three-Dimensional

AA – Aluminium Alloy

ASTM – American Society for Testing and Materials

CJP – Christopher James Patterson (model)

COD – Crack Opening Displacement

CTOD – Crack Tip Opening Displacement

$CTOD_p$ – Plastic Crack Tip Opening Displacement

DD3IMP – Deep Drawing 3D IMPlicit finite element solver

DIC – Digital Image Correlation

EPFM – Elasto-Plastic Fracture Mechanics

FCG – Fatigue Crack Growth

FCGR – Fatigue Crack Growth Rate

GRG2 – Generalised Reduced Gradient

LEFM – Linear Elastic Fracture Mechanics

NLC – Number of Load Cycles

PICC – Plasticity Induced Crack Closure

SS – Stainless Steel

1. INTRODUCTION

1.1. Motivation

Predicting unstable fracture or growth of a pre-existing crack is the most fundamental issue in fracture mechanics [1].

Fatigue is a very complex process affected by many factors [2], such as loading, geometry, material, environmental conditions, etc, and it is still the target of research for better understanding of the matter. It is composed of three phases, initiation, propagation of the cracks and final fracture. The total fatigue life is equal to the sum of the lives of the initiation and propagation phases, but in some of the cases, the time of propagation is much higher. Also, methodologies for structural dimensioning have been applied, which are based on the principle that cracks are present in structures arising from manufacturing processes, etc. These new methodologies change the expected life of the components because it is assumed that the cracks already exist and crack propagation requires lower levels of stress than crack initiation.

Most studies of fatigue crack propagation have been devoted to understanding the effect of loading parameters, and several models have been proposed, namely by Paris and Erdogan [3], Erdogan and Ratwani [4], Hartman and Schijve [5]. The study of the effect of material parameters on FCG rarely has been addressed in the literature. In fact, it is difficult to develop parametric experimental studies focused on material properties, because these cannot be changed one by one. On the other hand, the numerical tools available, namely Nasgro [6], are mainly devoted to the study of loading parameters.

Typically, the service life of components is determined with da/dN-ΔK curves. Some inconsistencies and limitations are pointed to this methodology. To overcome this aspect other methodologies were proposed, like crack closure concept, T-stress, CJP model, integral J, energy dissipated at the crack tip, CTOD, etc. This study follows the methodology proposed by Antunes *et al*. [7] based on plastic CTOD. This nonlinear parameter is supposed to be able to quantify the plastic deformation at the tip, which is

linked to the propagation of the crack. It includes crack closure and excludes the elastic deformation, which is not expected to contribute to fatigue crack growth. The da/dN versus plastic CTOD opened an opportunity to develop numerical parametric studies focused on the effect of loading, geometrical and material properties.

As such, this study is focused on the study of the effect of material properties on the propagation of the fatigue cracks.

1.2. Objectives

The main objective of this work is to study the effect of the elasto-plastic parameters of the material on fatigue crack growth. As specific objectives it is possible to point out:

- Identify the parameters that characterize the elasto-plastic material behaviour;
- Define materials to study the effect of different parameters;
- Study the effect of each parameter on plastic CTOD, and crack closure;
- Compare obtained relationships with models proposed in the literature;
- Study the sensitivity of each elasto-plastic property in plastic CTOD range, for each material.

1.3. Layout of the thesis

This thesis is divided into seven chapters. The numbering and presentation of each chapter are performed as follows:

• Chapter 1, Introduction: the motivation and presentation of the matter in question are made. The objectives and outline of the thesis are presented.

• Chapter 2, The literature review: some notions of fatigue theory are shown. The issues regarding da/dN-ΔK are explained as well as the methodology followed in this work.

- Chapter 3, Material model: some notions of plasticity theory are presented. Elasto-plastic parameters and the hardening laws are identified.
- Chapter 4, Numerical model: it is defined the physical situation, the model used for the specimen, and the finite element discretization. The software employed is presented.
- Chapter 5, Numerical results: in this chapter, the effect of the elasto-plastic parameters on fatigue crack growth is studied.
- Chapter 6, Discussion: a sensitivity analysis between δ_p and the elasto-plastic properties is performed.
- Chapter 7, Conclusions: the main conclusions obtained in this work are presented. Some proposals are suggested for future works.

2. LITERATURE REVIEW

2.1. Fatigue phenomenon

According to ASTM [8], fatigue is defined as a process of progressive and localized plastic deformation occurring in a material subjected to cyclic stresses and strains at high-stress concentration locations that may culminate in cracks or complete fracture after a sufficient number of fluctuations.

Time-varying loads are the most common in machinery elements. Therefore, these elements are likely to fail in service due to breakages designated as fatigue failures. Fatigue can be understood as a progressive weakening phenomenon of a metal when subjected to dynamic loads, that is responsible for 80% to 90% of all parts failure operating at ambient temperature [9].

Assuming that there are no cracks present in a part, the fatigue process comprises three phases:

1. Crack initiation: occurs at the surface of the part, because crystalline grains at the surface are more prone to deformation, namely plastic deformation, or at high-stress concentrations zones (notch, etc). Nucleation and subsequent microscopic growth of the crack follow the appearance of slip lines with a high density of dislocations, irreversible and oriented 45º in relation to the loading direction. The presence of microstructural barriers is responsible for slow crack growth;
2. Crack propagation: sliding planes begin to be created adjacent to the slit end, and the displacement begins to occur in a direction perpendicular to the load application. At this stage, while maintaining the request, there is a progressive increase in the crack propagation speed.
3. Final fracture: is characterized by an increase of the speed of propagation and the crack becomes unstable. When the remaining material can no longer tolerate the stresses or strains, sudden fracture occurs.

2.2. LEFM concepts

LEFM is a theory proposed by Irwin [10], in 1958 and was originally developed to describe fracture behaviour. Later was extended to fatigue crack growth behaviour and damage-tolerant design. It has as a basic assumption that material conditions are predominantly linear elastic during the fatigue process.

A crack subjected to loads tends to behave like a notch in a material, i.e., as a stress concentration zone, due to the geometry of the crack. These stresses potentiate the appearance of a zone where plastic deformation occurs at the front of the tip, shown and discussed ahead. Following the LEFM, the plastic deformation is not accounted for [11] and the damage at the crack tip is assumed to be controlled by the elastic field [12].

The stress intensity factor, K, is the main parameter responsible for the elastic field and deformations in the surroundings of the crack tip in monotonic conditions and it is supposed to control the FCG. The stress intensity factor is given by:

$$K = Y\sigma\sqrt{\pi a}, \tag{2.1}$$

where Y is a geometric factor, σ is the nominal stress applied and a the crack length.

In cyclic loading, the stress intensity range, ΔK, can be quantified by:

$$\Delta K = K_{max} - K_{min}, \tag{2.2}$$

where K_{max} and K_{min} are the maximum and minimum stress intensity factor, respectively.

In order to perform life predictions for FCG, this theory employs crack growth rate, da/dN -ΔK curves, as schematically shown in Figure 2.1. Information about fracture toughness, K_{1C} (K_C), initial crack size, a_0, stress intensity factor, K, maximum, and minimum stresses, σ_{max} and σ_{min} , respectively are needed to represent these curves. Three regions can be identified in these curves:

- Threshold region: there is no crack propagation for values below fatigue threshold, ΔK_{th}. When ΔK_{th} is reached, there is a quick increase of da/dN with ΔK. ΔK_{th} can be determined experimentally.
- Paris region: linear increase of da/dN with the increase of ΔK, in logarithmic scales, described by Paris and Erdogan law [3]:

$$\frac{da}{dN} = C(\Delta K)^m, \tag{2.3}$$

in which C and m are material constants that depend on the material, environmental conditions and stress ratio.

Paris' law is generally accepted for a wide range of different materials, however, the physical meaning is limited. A major issue is how to explain stress ratio effects [13].

- Accelerated region: when K_{max} takes values close to K_{1C} (K_C), a sudden increase in da/dN occurs until the final fracture. This regime does not always happen, as it is the case of materials with high ductility.

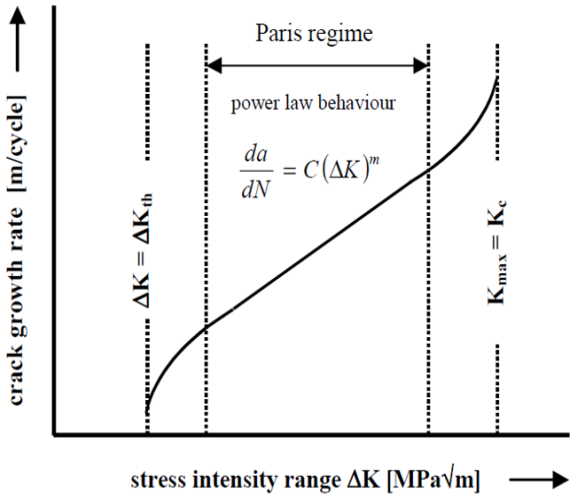

Figure 2.1. da/dN versus ΔK curve on log-log scale. Adapted from [14].

2.3. Issues regarding LEFM

As previously said, ΔK is the parameter that controls FCG at the crack tip in LEFM theory. The use of this methodology has some advantages, such as K can be obtained numerically, many solutions already exist in the literature for different cracked geometries, for long cracks LEFM gives good results and the linearity evidenced by Paris law is much appreciated.

Several problems have however been pointed out to this methodology, such as inability to predict the influence of stress ratio and load history on $\mathrm{da/dN}$ -ΔK relations, the odd behaviour observed for short cracks, the validity limited to LEFM [15] and the dimensional problems in the curves in question, as can be analysed from the equation 2.3 where the units of $(\Delta \mathrm{K})^{\mathrm{m}}$ and $\mathrm{da/dN}$ are $\left[\mathrm{MPa}\sqrt{\mathrm{m}}\right]$ and $\left[\frac{\mathrm{m}}{\mathrm{cycle}}\right]$, respectively, which causes constant C to have units of $\left[\frac{\sqrt{m}}{MPa \cdot cycle}\right]$.

In fact, local plasticity at the crack tip controls both fracture and crack growth, i.e., FCG is linked to non-linear and irreversible mechanisms happening at the crack tip. LEFM is only valid in small-scale crack tip yielding which is controlled by the plastic zone size to crack length ratio and the magnitude of operating stress.

2.4. Some proposed solutions

Different theories have emerged to try to fulfil the gaps resulting from the application of LEFM theory to fatigue crack propagation. One of the most known is the crack closure phenomenon. Elber [16] demonstrated the importance of this phenomenon by observing that even in tensile load a fatigue crack could be closed, which explains how stresses lower than a crack opening stress can be insufficient to propagate the crack. The contact of the crack faces has a protective effect at the tip, and it is assumed that only the portion of the load cycle during which the crack is open contributes to crack propagation [17]. The effective stress intensity range, $\Delta \mathrm{K_{eff}}$, is then given by:

$$\Delta K_{eff} = K_{max} - K_{open}, \tag{2.4}$$

where $\mathrm{K_{open}}$ is the stress intensity factor below which the crack remains closed.

In Figure 2.2 is represented the effective stress intensity range and the relevant stress intensity factors.

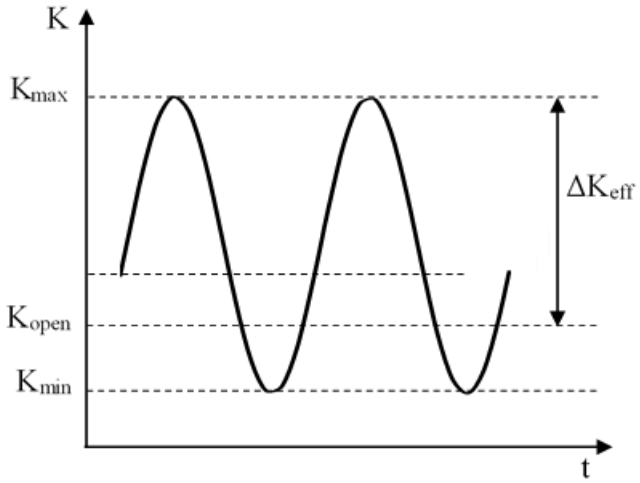

Figure 2.2. Schematic representation of the effective stress intensity factor. Adapted from [17].

Regarding $\mathrm{da/dN}$ -ΔK curves, in the Paris equation, ΔK should be replaced by ΔK_{eff}, as follows:

$$\frac{da}{dN} = C\left(\Delta K_{eff}\right)^{m}. \tag{2.5}$$

Different crack closure mechanisms emerged, such as plasticity-induced [18], (PICC), oxide-induced [19] and roughness-induced [20].

Although the crack closure concept has provided a better understanding of the effect of variables like load history and microstructure, some new issues have arisen with this concept, and its importance in FCG rate is not consensual in the scientific community

New approaches were proposed in order to mitigate the problems associated with fatigue theory. T-stress concept was used to quantify the effect of specimen's geometry on crack closure. Partial crack closure states that the contact of crack flanks does not happen immediately behind the crack tip, which implies the existence of a contribution of the load spectrum below crack closure for fatigue damage. CJP model describes the stress field around the crack tip using four different parameters.

All the methodologies referred above are based on ΔK, but due to the limitations associated with this elastic parameter to measure what happens at the crack tip, nonlinear parameters were proposed to replace ΔK.

2.5. Elasto-plastic fracture mechanics

Under cyclic loadings, three induced zones are developed at the crack tip. The representation of these zones, in mode I of loading (traction), are represented in Figure 2.3.

Each zone can be characterized as follows:

- Zone I: It is called the "cyclic plastic zone" and it is distinguished by a hysteresis loop in stress-strain plots. The shape of the loop is affected by the stress ratio and ΔK.
- Zone II: known as monotonic plastic zone. During loading, plastic deformation is achieved. When the specimen is unloaded, an elastic charge-discharge occurs.
- Zone III: is the most distant zone of the tip. In this region, the material has an elastic behaviour.

Depending on the stresses developed at the crack tip, the plastic zone size varies. The stress state of the material also has an influence on the size of the plastic zone. In plane stress conditions, plastic zone size is bigger than in plane strain conditions. This is due to the normal stress component, σ_Z, which in plane stress conditions is equal to zero, but in plane strain conditions assumes positive values (traction), restricting plastic flow.

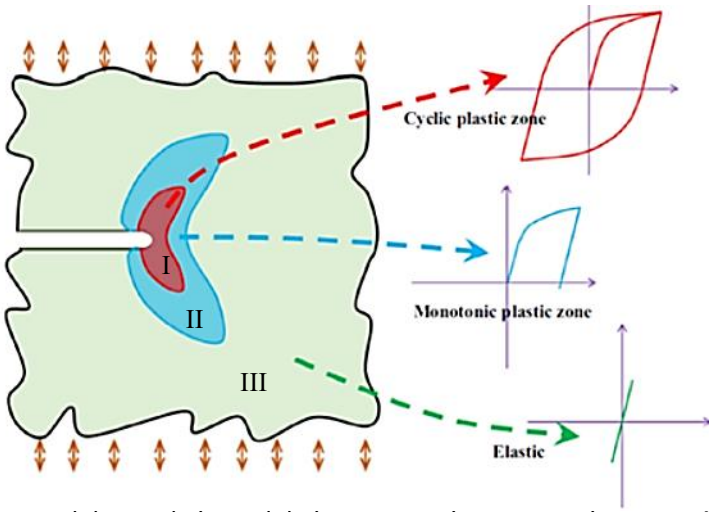

Figure 2.3. Induced zones, around the crack tip, and their responses in stress-strain curves. Adapted from [21].

Some nonlinear parameters were proposed for a better understanding and measurement of the phenomena happening at the tip. The more relevant parameters are the

plastic deformation range $(\Delta\varepsilon_{p,yy})$, the radius of inverse plastic zone (r_{pc}), the total plastic dissipation by cycle and the crack tip opening displacement (CTOD).

As the present study is based on the CTOD, only this parameter will be developed next.

2.5.1. CTOD

It was proposed by Wells [22] in 1961 as a measure of fracture toughness by noticing that the crack faces moved apart prior to fracture in test specimens which exhibited a high degree of plasticity [23]. This parameter is herefore the measurement of the displacement at the crack flanks. The name COD (Crack Opening Displacement) is used for measures relatively distant from crack tip while CTOD (Crack Tip Opening Displacement) is used for measures relatively close to crack tip.

There are two definitions of the CTOD concept, as shown in Figure 2.4. The first, measures the opening displacement of the original crack tip. The other, proposed by Rice, measures the displacement at an intersection of a 90º vertex with the crack flanks. These two definitions are equivalent if the crack blunts in a semicircle.

The accurate measuring of CTOD is very important because an underestimate can cause unstable propagation and ultimately a failure. On the other hand, an overestimate can cause size defects to be very small, increasing the inspection intervals. To overcome this aspect, the measuring of CTOD is, typically, performed numerically with finite element method rather than experimental testing. Also, the evaluation of CTOD is done at the first node behind the crack tip.

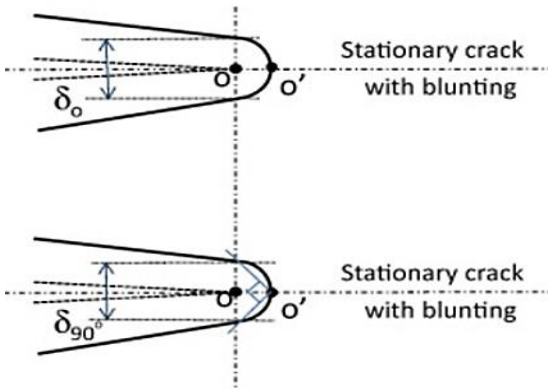

Figure 2.4. Definitions of CTOD [24].

Some relations have been proposed using CTOD. By micrography, Pelloux [25] proved that the CTOD concept allowed predicting the spacing of the fatigue striations and, consequently, the crack growth rate. Otherwise, Bates and Santhanam [26] linked CTOD with the deformation at the notch end:

$$CTOD = 0{,}103 \cdot \varepsilon_{p,yy}, \tag{2.6}$$

where $\varepsilon_{p,yy}$ corresponds to the total plastic deformation, according to the vertical direction, ie perpendicular to the direction of loading. In 1994 Nicholls [27] assumed a polynomial relation between crack growth rate and CTOD:

$$\frac{da}{dN} = b\ (CTOD)^{1/p}, \tag{2.7}$$

being b and p constants. Nicholls also proposed:

$$CTOD = \frac{\lambda K^2}{E\sigma_{ys}}, \tag{2.8}$$

where K is the stress intensity factor, E and σ_{ys} are the Young´s modulus and yield stress of the material, respectively and λ a constant.

Tvergaard [28] and Pippan and Grosinger [29] indicated a linear relation between da/dN and CTOD for very ductile materials, being c a constant:

$$\frac{da}{dN} = c \times CTOD. \tag{2.9}$$

More recently Antunes *et al*. [7] proposed the replacement of ΔK by $CTOD_p$ in da/dN curves to overcome the issues linked to LEFM.

Some proposals have been made in the prediction of da/dN using this methodology.

For AA7050-T6 [30]:

$$\frac{da}{dN} = 0.5246 \times \delta_p. \tag{2.10}$$

For SS304L [31]:

$$\frac{da}{dN} = 0.003374 \times \delta_p^3 + 0.014074 \times \delta_p^2 - 0.000047 \times \delta_p. \tag{2.11}$$

For AA2050-T8 [15]:

$$\frac{da}{dN} = 0.2407 \times \delta_p^2 + 0.4154 \times \delta_p. \tag{2.12}$$

2.6. Work already done based on CTOD

The research group developed different studies based on plastic CTOD, namely:

- study the effect of numerical parameters on the values of plastic CTOD range, δ_p.
- propose the da/dN versus $\Delta CTOD_p$ approach, as an alternative to classical da/dN-ΔK curves. Prove the competence of this approach.
- Obtain results for different materials and compare the curves. The materials studied were the AA6082-T6 [32], AA7050-T6 [30], AA2050-T8 [15], 18Ni300 steel [33], 304L stainless steel [31].
- Show that the da/dN-$\Delta CTOD_p$ approach can be used to predict the effect of stress ratio, stress state, and variable amplitude loading. The predictions follow well-known experimental trends [31].
- Prove that the da/dN-δ_p model can be determined only experimentally, using DIC to measure the CTOD.

The elastic regime was also used to:

- Predict fatigue threshold [34].
- Correct da/dN- ΔK_{eff} curves, subtracting the elastic range of load [35].

The objective here is to extend this work, using the prediction capabilities of da/dN-δ_p approach to study the effect of material properties on FCGR.

3. MATERIAL MODEL

3.1. Plasticity theory

The correct modelling of the elastic-plastic behaviour of the materials is very important in numerical simulations so that the predictions made are as precise as possible.

Crystallographic and phenomenological constitutive models describe and predict the elastic-plastic behaviour of metal materials. The first, represent the microscopic theory of plasticity and assumes that the material is constituted by one or several crystals forming a crystalline body. The second, represent the macroscopic theory of plasticity, which assumes that the material is homogeneous and is only valid at temperatures for which thermal phenomena may be neglected. This theory is capable of predicting the distribution of stresses and strains in polycrystalline metals, not only in situations where the elastic and plastic strains are of comparable magnitudes but also in situations where the plastic strains are large enough for the elastic strains to be disregarded [36].

Phenomenological constitutive models are usually constituted by:

- Yield criterion, governing the limit of the elastic behaviour under any combination of applied stresses.
- Hardening law, to describe how the yield surface evolves during plastic deformation.
- Plastic flow rule, which provides a relationship between the state of stress and the plastic deformation increment.

A constitutive model can be described by a function of $\mathcal{F}$:

$$\mathcal{F}(\boldsymbol{\sigma}' - \boldsymbol{X}, \bar{\varepsilon}^p, \alpha, \beta) = \bar{\sigma}(\boldsymbol{\sigma}' - \boldsymbol{X}, \alpha) - Y(\bar{\varepsilon}^p, \beta), \tag{3.1}$$

$\bar{\sigma}(\boldsymbol{\sigma}' - \boldsymbol{X}, \alpha)$ is the equivalent stress, which is given by a yield criterion and $Y(\bar{\varepsilon}^p, \beta)$ represents the evolution of the yield stress during the deformation, according to the hardening law employed. The equivalent stress $\bar{\sigma}(\boldsymbol{\sigma}' - \boldsymbol{X}, \alpha, \beta) = \bar{\sigma}$ has as variables, $\boldsymbol{\sigma}'$, the deviatoric Cauchy stress tensor and $\mathbf{X}$, the deviatoric back-stress tensor. The portion $Y(\bar{\varepsilon}^p) = Y$ represents the flow stress and depends on the equivalent plastic strain, $\bar{\varepsilon}^p$. Lastly, α and β represent the material parameters of the constitutive model [37].

The yield surface, in Cauchy´s principal stress space, is represented in Figure 3.1. This surface consists of a cylinder varying its surface according to the criterion in study. Tresca criterion is characterized by a hexagonal yield surface, on the other hand, the Von Mises criterion is featured by an elliptical surface.

Yielding occurs when the equivalent stress equals the flow stress. Therefore, the limit of the elastic regime can be expressed by:

$$\mathcal{F} = \bar{\sigma} - Y = 0 \iff \bar{\sigma} = Y. \tag{3.2}$$

Inside the yield surface, any stress state of the material complies the relation $\bar{\sigma}<Y$, occurring only elastic deformation. The associated flow rule states that the increment of the plastic strain tensor is normal to the yield surface.

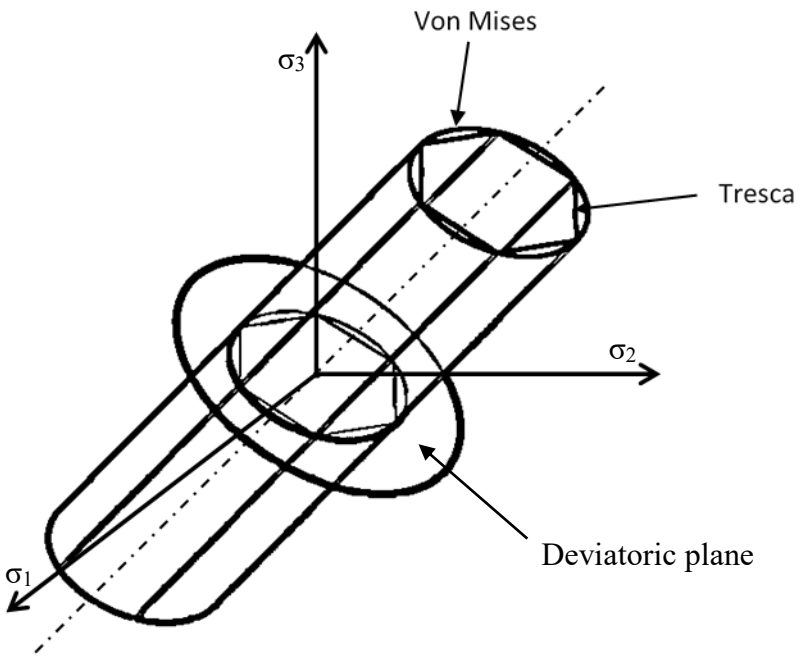

Figure 3.1. Representation of the yield surface, in Cauchy´s principal stress space.

The surface axis is equally inclined to the main axes, in such a way that it represents the condition $\sigma_1=\sigma_2=\sigma_3$. Points located along this axis, represent purely hydrostatic states of stress which do not have any influence on the yielding.

The plan $\sigma_1+\sigma_2+\sigma_3=0$, known as the deviatoric plane, is perpendicular to the surface axis and contains the origin of the coordinates.

3.2. Yield criteria

The onset of elastic deformation is measured by a stress value, known as yield stress. This stress is often obtained by performing a uniaxial test. Since most structures are subjected to multiaxial stresses, the yield stress is used in a multiaxial measure of yielding called yield criterion.

There are two commonly used yield criteria, Tresca [38] and Von Mises criterion [39]. Tresca criterion postulates that, for metallic materials, yielding occurs when maximum shear stress reaches the value it has when yielding occurs in the tensile test and is given by:

$$max\{|\sigma_1 - \sigma_2|, |\sigma_1 - \sigma_3|, |\sigma_2 - \sigma_3|\} = \sigma_0. \tag{3.3}$$

Due to the existence of angular points in the yield surface, Tresca´s criterion poses mathematical difficulties in solving some problems. Therefore, Von Mises replaced the hexagonal prism with the circumscribed cylinder. Von Mises criterion is the most widely used, in which yielding occurs when effective stress reaches the yield value defined and can be written as follow:

$$(\sigma_1 - \sigma_2)^2 + (\sigma_1 - \sigma_3)^2 + (\sigma_2 - \sigma_3)^2 = 2{\sigma_0}^2. \tag{3.4}$$

3.3. Strain-hardening plasticity

Strain hardening can be perceived by a tensile test. Figure 3.2 shows a true stress-strain curve for AA5083. After passing the elastic limit, point A, the material undergoes plastic flow. Further increases in load are required to maintain the plastic flow and an increase in displacement, this phenomenon is known as strain-hardening. If the specimen is unloaded at point B, it will return along the path BC, parallel to the original elastic limit, showing elastic recovery. The strain that remains after unloading is called plastic deformation, which is permanent. If the material is now loaded again, the stress-strain curve will retrace the unloading path CB until it again reaches the plastic state. Further increases in stress will cause the curve to follow BD .

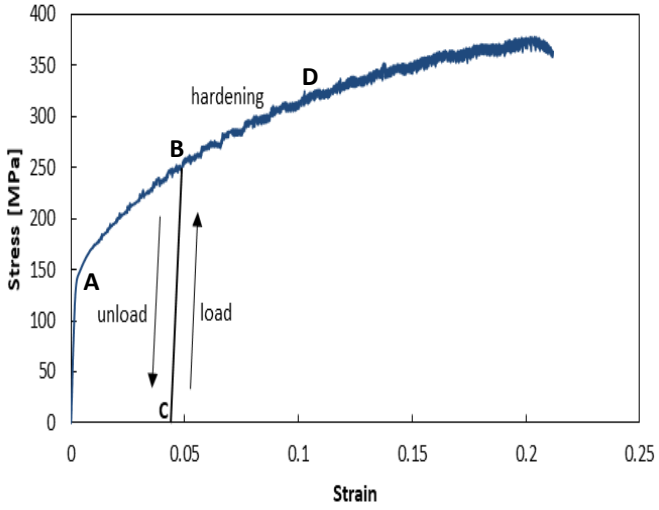

Figure 3.2. Stress-Strain curve showing strain hardening phenomenon.

There are essentially two types of hardening laws, isotropic and kinematic.

3.3.1. Isotropic hardening

The isotropic hardening model is the most widely used hypothesis for strain hardening. This law assumes that the yield surface increase in size during continued plastic deformation without a change in shape (homothetic expansion), as represented in Figure 3.3. Therefore, the yield surface is uniquely defined by the final plastic state of stress regardless of the actual strain path [40]. According to this law, the material remains isotropic throughout the deformation, and the Bauschinger effect is absent.

Some metallic materials present stress saturation at large deformations. For this reason, models, like Voce [41], were developed. Voce law can be written as follow:

$$Y = Y_0 + (Y_{Sat} - Y_0)[1 - exp(-C_Y \bar{\varepsilon}^p)], \tag{3.5}$$

where Y_0 is the yield stress, Y_{Sat} is the isotropic saturation stress, C_Y is a parameter of the Voce law that gives information as the isotropic saturation stress is reached more or less rapidly and $\bar{\varepsilon}^p$ is the equivalent plastic strain.

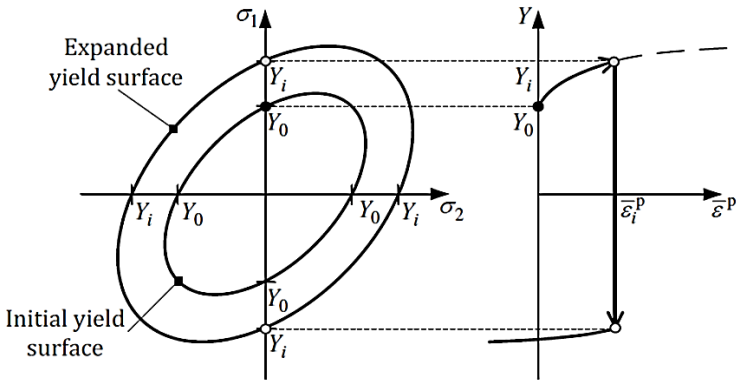

Figure 3.3. Representation of the evolution of the yield surface in isotropic hardening, on the left and, on the right side the corresponding stress vs plastic strain curve. Adapted from [37].

3.3.2. Kinematic hardening

The kinematic hardening model proposes a rigid translation of the yield surface, without a change in shape and size, see Figure 3.4. This model is recommended for describing plastic deformation under strain path changes and is capable to predict the development of anisotropy and Bauschinger effect. This phenomenon consists in the reduction of the yield stress in compression after a tensile load, or vice versa, and shows that the hardening is oriented (the increase of the yield stress due to a previous tensile strain does not mean that in a subsequent compression the same is verified) and is an example of how the history of deformation influences the plastic behaviour of metallic materials.

A non-linear kinematic model was proposed by Armstrong & Frederick [42], which can be written:

$$\dot{\boldsymbol{X}} = C_X \left[\frac{X_{Sat}}{\bar{\sigma}} (\boldsymbol{\sigma}' - \boldsymbol{X}) - \boldsymbol{X} \right] \dot{\bar{\varepsilon}}^p, \tag{3.6}$$

where C_X is a parameter of the Armstrong & Frederick law and as a similar purpose as C_Y in equation 3.5, but regarding kinematic saturation stress, X_{Sat} is the kinematic saturation stress, $\bar{\sigma}$ is the equivalent stress and $\dot{\bar{\varepsilon}}^p$ is the equivalent plastic strain rate.

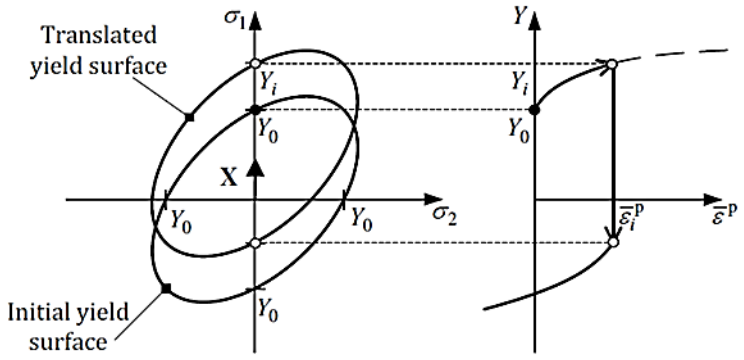

Figure 3.4. Representation of the evolution of the yield surface in kinematic hardening, on the left and, on the right side the corresponding stress vs plastic strain curve. Adapted from [37].

3.4. Materials studied

In this study were considered two materials, an SS304L, and the AA7050-T6. For the particular case of the study of the effect of Young´s Modulus on FCG, the AA2050-T8 was also considered. A plane stress state was assumed for all materials.

The SS304L has austenitic and non-magnetic microstructure, with a composition of Chromium (min 18.0%) and Nickel (min 8%), thus known as "18-8". It has good corrosion resistance since the alloying elements are present in a single phase, as well as good ease in cold forming and welding, however, the hardening is superior to most unalloyed steels [43]. It is commonly used in the plant for the manufacture and storage of nitric acid, at concentrations below 65% [44] and in the automotive and aerospace areas.

The AA 7050-T6 is an aluminium alloy belonging to 7000 series (Zn-alloyed). This series family is characterized by having very high strength and high toughness. Relative to the microstructure, Zn is dissolved in solid solution and precipitated out as coherent submicroscopic particles. It is solution-treated and aged to increase strength. Zn and Mg allow to maximize age-hardening potential and is very used in the aerospace industry due to high specific resistance.

AA 2050-T8 belongs to 2000 series (Cu-alloyed) and it also contains lithium. This type of alloys are known for their benefits in reducing density and increasing Young´s modulus, proportionally to their Li content. The AA 2050-T8 was defined for a medium to high strength and high damage tolerance alloy intended to out-perform the property balance of 2xxx thin plate alloys and 7xxx thick plate alloys [15].

3.5. Identification of elasto-plastic constants of the materials

An optimization procedure was performed to identify the material parameters that best describe the plastic behaviour of the materials. The identified set of material parameters was obtained by minimization of the least-squares cost function F(**A**):

$$F(\boldsymbol{A}) = \sum_{i=1}^{N} \left(\frac{\sigma^{Fit}(\boldsymbol{A}) - \sigma^{Exp}}{\sigma^{Exp}} \right)_i^2, \quad (3.7)$$

where $\sigma^{Fit}(\boldsymbol{A})$ and σ^{Exp} are the fitted and the experimentally measured values of true stress, respectively; **A** is the set of Voce and Armstrong & Frederick parameters that minimises $F(\mathbf{A})$; N is the total number of experimental points. The minimization of F(**A**) was performed using the GRG2 algorithm [45], included in the Microsoft Excel Solver tool. More information about the fitting of the numerical curves, the total number of experimental data points and the low-cycle fatigue tests made, for each material, can be found in the references in Table 3.1.

The constants values that better represent the cyclic plastic behaviour are indicated in Table 3.1. These values enable proper numerical modelling of the behaviour displayed experimentally by the materials.

Table 3.1. Elastic-plastic constants identified.

MATERIAL	***HOOKE´S LAW***		***VOCE HARDENING LAW***			***ARMSTRONG-FREDERICK LAW***	
	E [GPa]	v [-]	Y_0 [MPa]	Y_{Sat} [MPa]	C_Y [-]	C_X [-]	X_{Sat} [MPa]
AA7050-T6 [30]	71.7	0.33	420.50	420.50	0	228.91	198.35
SS304L [31]	196	0.30	117.00	204.00	9	300.00	176.00
AA2050-T8 [15]	77.4	0.30	383.85	383.85	0	97.38	265.41

.

4. NUMERICAL MODEL

4.1. Physical situation

The numerical tests were performed with a C(T) (Compact-Tension) specimen illustrated in Figure 4.1. The specimen had a width, W, of 50 mm, an initial crack length, a_0, of 24 mm, therefore a_0/W is 0.48. The thickness of the specimen was 12 mm, in the experimental study of SS304L.

In the study of the effect of Young's modulus was also considered an M(T) (Middle-Tension) specimen, for 2050-T8 aluminium alloy (AA2050-T8), with a width of 160 mm and an initial crack length, a_0, of 15 mm. The geometry and size of the specimens are in accordance with ASTM E647 standard [8].

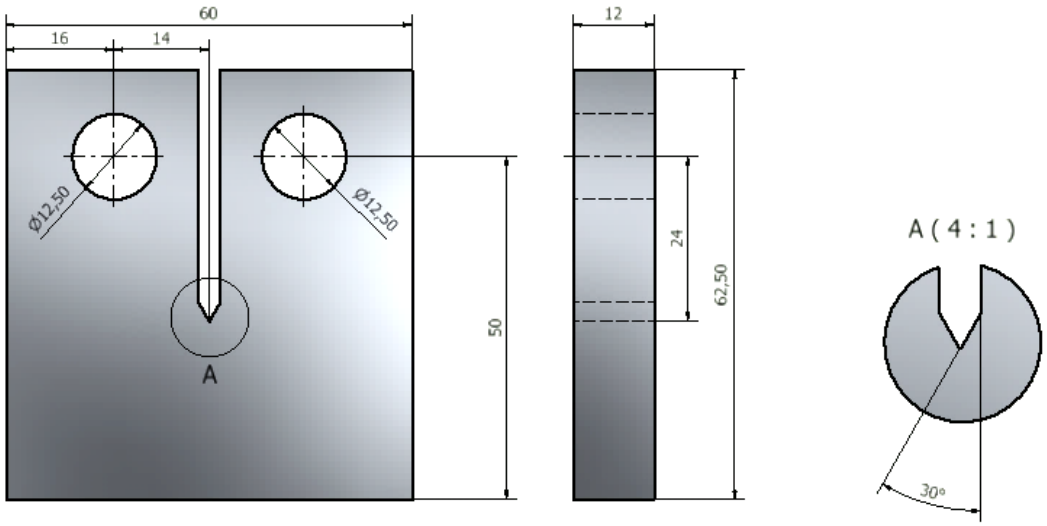

Figure 4.1. Physical C(T) specimen.

4.2. Physical model

Since the C(T) specimen has two planes of symmetry, only 1/4 of the specimen was modelled considering adequate boundary conditions, see Figure 4.2. The last node on the right end side of Figure 4.2(a) was fixed to avoid rigid body movement. Figure 4.2 (b)

shows a lateral view of the specimen with symmetry conditions for plane stress state. The load was applied at the hole, as indicated in Figure 4.3 (a). To reduce numerical effort only 0.1 mm of thickness was modelled.

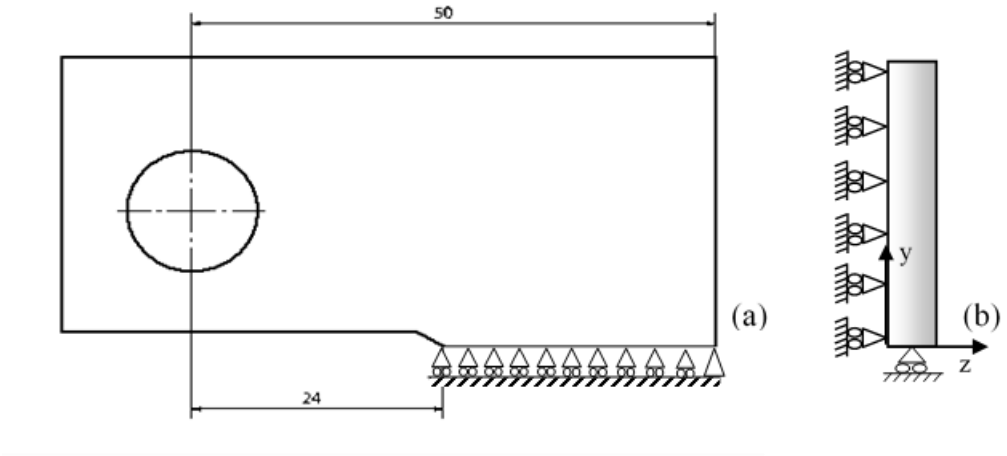

Figure 4.2. (a) Model of the C(T) specimen; (b) Boundary conditions for plane stress state.

The elasto-plastic properties of the materials were identified in Table 3.1. Throughout this work, several changes were made to these properties to study their effect on FCG. These variations are in Table 4.1.

Table 4.1. Variations of the elasto-plastic properties.

Material	Hooke's law		Voce hardening law			Armstrong-Frederick law	
	E [GPa]	v [-]	Y_0 [MPa]	Y_{Sat} [MPa]	C_Y [-]	C_X [-]	X_{Sat} [MPa]
AA7050-T6							
0.50E	35.85						
0.75E	53.78						
1.25E	89.63						
1.50E	107.58						
0.50Y_0			210.25	210.25			
0.75Y_0			315.38	315.38			
1.25Y_0			525.63	525.63			
1.50Y_0			630.75	630.75			
0.50X_{Sat}							99.18
0.75X_{Sat}							148.76
1.25X_{Sat}							247.94
1.50X_{Sat}							297.53
0.50C_X						114.46	
0.75 C_X						171.68	

1.25 C_X				286.14	
1.50 C_X				343.37	
SS304L					
0.50E	98				
0.75E	147				
1.25E	245				
1.50E	295				
0.50Y_0		58.50			
0.75Y_0		87.75			
1.25Y_0		146.25			
1.50Y_0		175.50			
0.50X_{Sat}					88.00
0.75X_{Sat}					132.00
1.25X_{Sat}					220.00
1.50X_{Sat}					264.00
0.50C_X				150.00	
0.75 C_X				225.00	
1.25 C_X				375.00	
1.50 C_X				450.00	
0.50Y_{Sat}			117.00		
0.75Y_{Sat}			153.00		
1.25Y_{Sat}			255.00		
1.50Y_{Sat}			306.00		
0.50C_Y			4.50		
0.75 C_Y			6.75		
1.25 C_Y			11.25		
1.50 C_Y			13.50		
AA2050-T8					
0.50E	38.70				
0.75E	58.05				
1.25E	96.75				
1.50E	116.10				

4.3. Finite element model

4.3.1. Finite element mesh

The finite element mesh, illustrated in Figure 4.3, comprised 7287 3D linear isoparametric elements and 14918 nodes. At the crack tip, the mesh was refined having square elements with 8×8 μm^2 to simulate strain gradients and local stress. A coarser mesh was used in the remaining volume of the body to reduce computational overhead. Along the thickness, only one layer of elements was used.

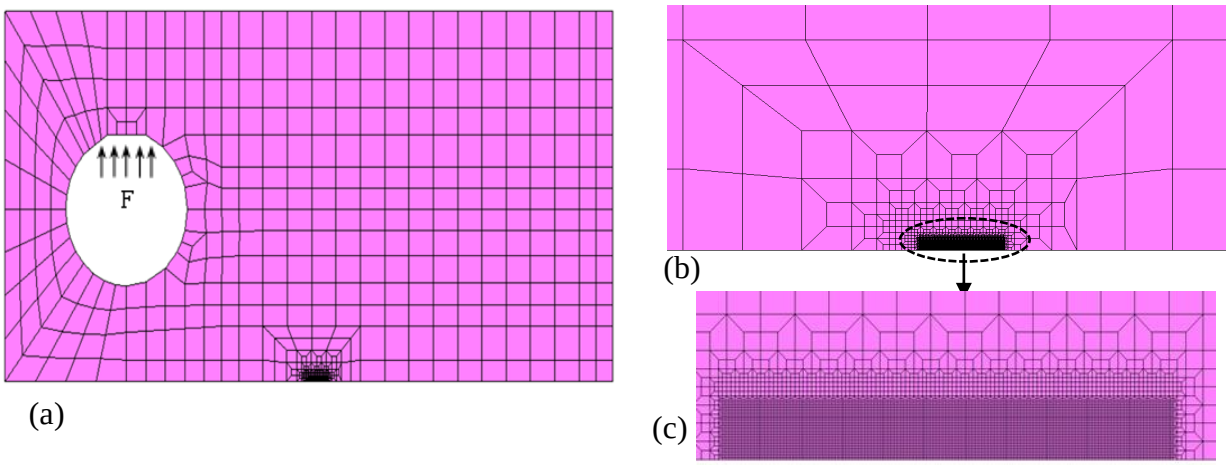

Figure 4.3. (a) Mesh of the C(T) specimen model; (b) and (c) Details of finite element mesh.

4.3.2. Crack propagation

Crack propagation was simulated by successive debonding at minimum load of both current crack front nodes. Two load cycles were applied between each crack increment corresponding to one finite element. A total number of 320 load cycles were performed, corresponding to a crack advance of $\Delta a = (160\text{-}1) \times 8 = 1272$ μm, since in the first block there was no crack propagation. The simulations are done with 159 crack propagations in order to stabilize crack tip fields and crack closure level, and therefore to obtain stable values of CTOD.

To eliminate crack closure phenomenon, in some numerical simulations the contact of crack flanks was removed.

4.3.3. Load

The numerical simulations had a cyclic load of constant amplitude, as indicated in Figure 4.4 with maximum and minimum values of 41.67 and 4.167 N, respectively and K_{max}, K_{min} and ΔK were 18.3, 1.83 and 16.5 MPa.m$^{0.5}$, respectively. In the particular case of the AA2050-T8, the maximum and minimum values were 641.28 and 64.13 N and K_{max}, K_{min} and ΔK were 48.88, 5.13 and 43.8 MPa.m$^{0.5}$ In all the cases the load ratio was R=0,1.

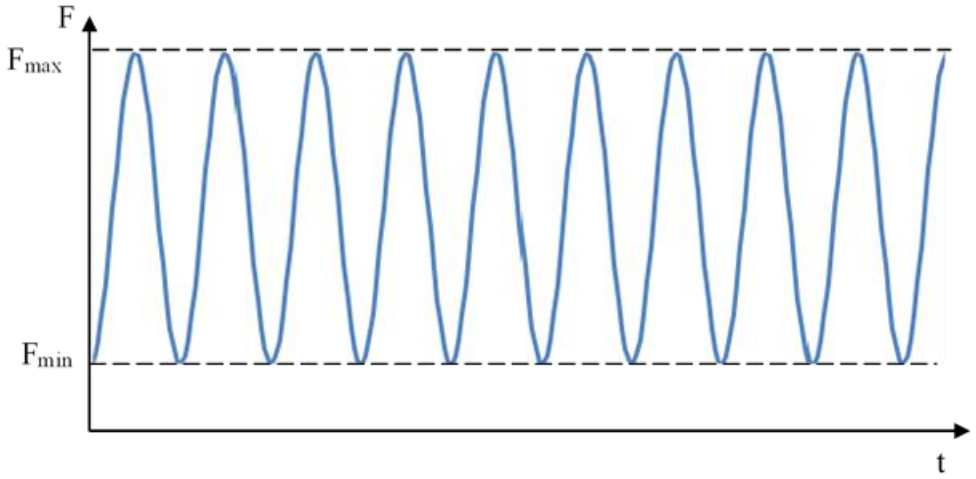

Figure 4.4. Representation of cyclic load applied.

4.4. Finite element software

The three-dimensional finite element software used to implement the numerical model was the DD3IMP in-house code, originally developed to simulate sheet metal forming processes [46]–[48]. This software takes into account large elastic-plastic deformations and rotations and assumes that the elastic strains are negligibly small with respect to unity. To simulate friction contact, the software uses the increased Lagrangian method. The nonlinear system obtained is solved with the Newton-Raphson method. The contact of the crack flanks is modelled considering a rigid body (plane surface) aligned with the crack symmetry plane.

In order to run the simulations, some information is required by the software. This information is given in "input" files.

- **Mesh.dat:** defines the discretization of the deformable body using finite elements: coordinates of each node, the connectivity of each element (i.e. the nodes that define the edges of each element) and the number of the material (missing information if only one material exists) [49];
- **mater1.dat:** contains information about the material properties (elastic properties, hardening law and yield criterion) used in the simulation. Whenever it is necessary to add a material to the simulation, a file with information related to the material in question is necessary;

- **phase.dat:** contains the loading conditions (magnitude of maximum and minimum loads, direction, etc.);
- **bcon.dat:** imposes the boundary conditions of the deformable body.
- **GaussPoints.dat:** defines the finite elements where the software record the values of stress and strain during the simulation;
- **Input.dat:** comprises all numeric parameters, such as convergence criterion, maximum number of iterations, tolerances, etc.);
- **Tool.dat:** defines the parametric surfaces.

The results of the simulations are given to the user in "output" files.

- **Nosfenda2.dat:** has information about the displacements of the nodes;
- **#enti1.res:** has the applied loads for each crack increment;
- **GPoint.dat:** contains the values of stress and strain for specific Gauss points and finite elements defined in file GaussPoints.dat;
- **Fcont.dat:** has the contact forces at minimum load;
- ***Bloco160*.ufo:** information about the last propagation of the crack.

4.5. Determination of relevant parameters

When the simulation ends, the last propagation of the crack (*Bloco 160*) is processed in an application developed in Visual Basic called PICC_v24a.exe. This application loads the Nosfenda2.dat and #enti1.res and generates a file called CTODvsLoad.dat which has the values of CTOD and load for the last propagation of the crack. These values of CTOD and load are then inserted in an Excel template named *Análise de Resultados CTOD* [50], which calculates the elastic and plastic CTOD ranges, and other parameters. This Excel template works in both contact and no contact simulations at the crack tip.

5. NUMERICAL RESULTS

5.1. CTOD versus load

Figure 5.1 (a) plots the crack tip opening displacement, i.e. CTOD, measured at the first node behind crack tip versus the applied load, F. This is a typical curve obtained in simulations with contact at the crack flanks. As can be seen, the crack remains closed between points A and B, although the increase of the load. Note that this curve was obtained after a crack growth of 1.272 mm, corresponding to 159 crack increments of 8 μm each. Above point B, the CTOD is no longer zero, which means that the crack opened. After the opening of the crack, a linear relationship is observed, between points B and C. In this load range, the crack presents a linear elastic behaviour. C is the point where the plastic CTOD equals 0.001 μm, which was the value defined empirically as the transition to elastic-plastic behaviour.

Plastic CTOD increases progressively between points C and D and reaches its maximum value at point D, corresponding to the maximum load. The total elastic and plastic ranges are identified as δ_e and δ_p, respectively, in Figure 5.1 (a). After point D, the load decreases and between D and G, a new linear relationship is observed, with a slope similar to that observed during loading. At point H the displacement reaches zero value, i.e., the crack closes.

Figure 5.1 (b) plots the total CTOD and the plastic CTOD ($CTOD_p$) versus the applied load. These are typical curves obtained in simulations without contact at the crack flanks. In this case, there is an overlap of crack flanks at minimum load. This is possible only in the numerical studies since it is not physically possible. The crack tends to open from the minimum load, unlike the case of Figure 5.1 (a), which means that both points A and B are coincident. Analogously to the previous figure, point C corresponds to the transition between the elastic and elastic-plastic regimes, while point D corresponds to the maximum load and maximum elastic and plastic strains. When the load decreases from its maximum value, a linear relationship is observed similar to that observed during loading. After point G, there is a non-linear relationship typical of the elastic-plastic regime, due to

reversed plastic deformation. In this type of simulation, there is no crack closure, therefore point H does not exist.

Figure 5.1 (b) also presents the plastic CTOD, which increases progressively with load after point C. The rate of variation also increases with load, which means that plastic deformation becomes easier. Reverse plastic deformation occurs during unloading, as already mentioned.

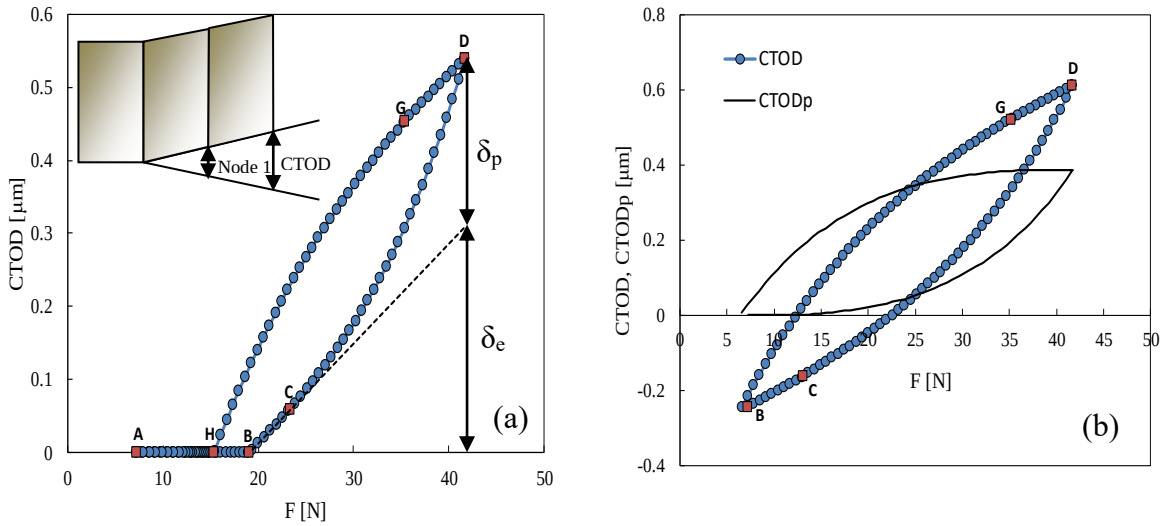

Figure 5.1. (a) CTOD versus load with contact; (b) CTOD and plastic CTOD versus load without contact (SS304L; plane stress; Δa=1.272 mm).

5.2. Effect of E without crack closure

Figure 5.2 (a) presents CTOD versus F for different values of Young's modulus. There is a significant effect of this elastic property on near-crack tip behaviour. The increase of rigidity decreases the deformation, i.e., the total CTOD range, as could be expected.

Figure 5.2 (b) shows the variation of plastic CTOD. After the elastic regime, there is a progressive separation of the curves and the material with lower E has the highest plastic CTOD range, δ_p.

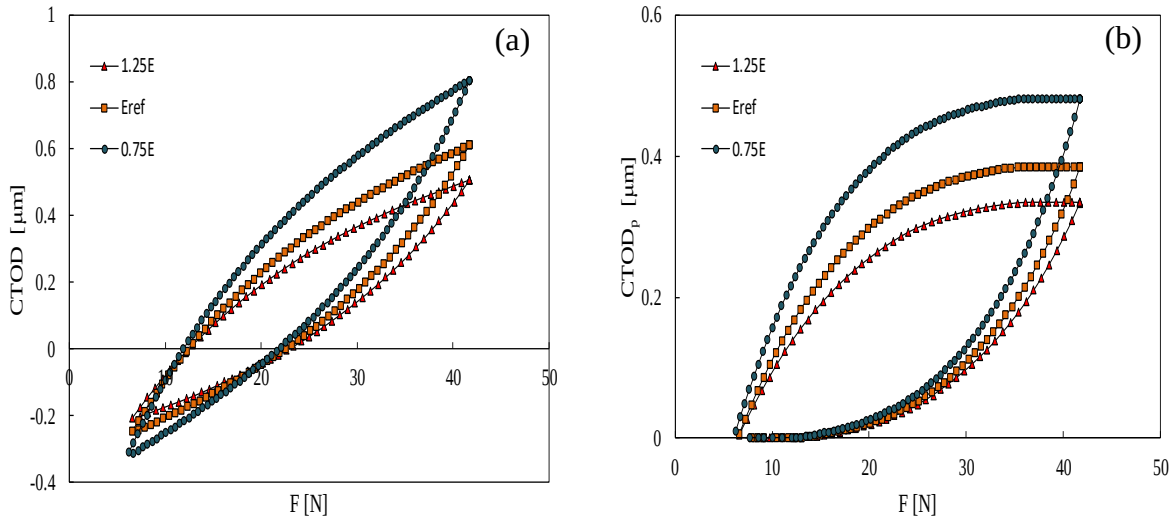

Figure 5.2. (a) CTOD versus load; (b) plastic CTOD versus load (SS304L; plane stress; no contact).

Figure 5.3 plots the plastic CTOD range (δ_p) versus 1/E, in plane stress state without contact of crack flanks. The points presented correspond to the five values of Young´s modulus indicated in Table 4.1, i.e. cases "0.50E", "0.75E", "Reference", "1.25E" and "1.50E". As it is shown, the increase of 1/E increase δ_p in all cases studied, i.e., the higher the E values, the lower the plastic CTOD range. Linear trendlines were added with excellent correlation coefficients for the cases without contact of crack flanks. The extrapolation to zero (i.e., to infinite E), does not give $\delta_p=0$, which may indicate some non-linearity for relatively low values of 1/E. The slope of the δ_p-1/E functions changes with the material. Linear relations between $CTOD_p$ and da/dN have been suggested in several experimental [51], numerical [30], [32] and analytical [51] studies. Therefore, the variations of Figure 5.3 are expected to correspond to linear relations between 1/E and da/dN. In other words, the results presented in Figure 5.3 agree with the relations proposed in the literature which assume that da/dN is proportional to 1/E (see Table B.1).

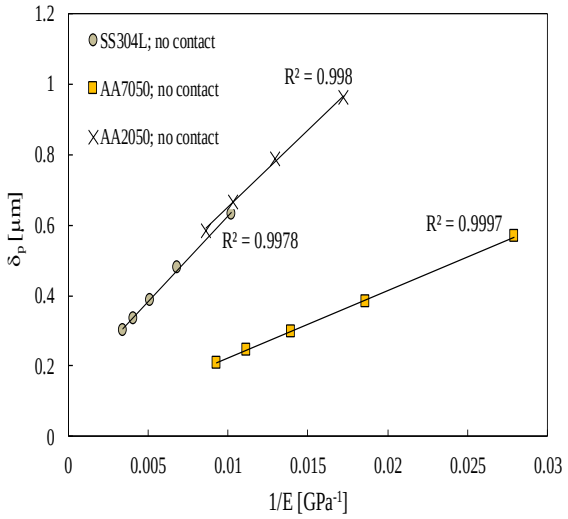

Figure 5.3. Plastic CTOD range, δ_p, versus the inverse of the Young´s modulus (plane stress, no contact of crack flanks).

Figure 5.4 (a) and (b) plot load versus $CTOD_p$ for SS304L and AA7050, respectively, in plane stress conditions. These results are similar to those presented in Figure 5.2 (b), but the axes were inverted and the curves were translated to a zero value of force, in order to facilitate the comparison. The objective is to study the material hardening at the crack tip, as a function of the Young's modulus. As it is shown, $CTOD_p$ increases with the increase of the applied load, and the rate of variation increases with the increase of the load level. In other words, the increase in plastic deformation increases its rate of variation. The increase of E reduces the level of plastic CTOD and also its rate of variation. In other words, the Young's modulus affects the material hardening at the crack tip.

Additionally, there is more difference between $CTOD_p$ for relatively lower values of E, than for relatively higher values of E, for which the curves are nearly coincident.

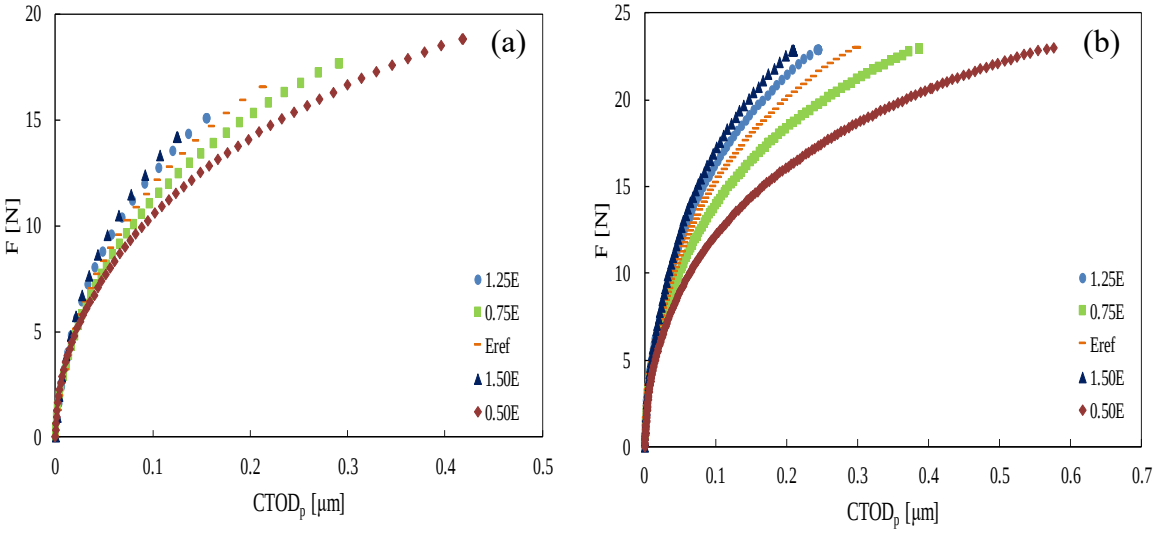

Figure 5.4. Load versus plastic CTOD. (a) SS304L; (b) AA7050-T6; plane stress (without contact, Δa=1.272mm).

It is important to explain the decrease of FCG with E, and the linear trend observed between δ_p and 1/E.

Figure 5.5 plots the plastic CTOD range, δ_p, versus the elastic CTOD range, δ_e. As can be seen, the increase of δ_e is accomplished by the increase of δ_p. The decrease of rigidity, i.e., the increase of 1/E, produces an increase of elastic deformation, and therefore an increase in plastic deformation. This explains the increase of FCG with 1/E.

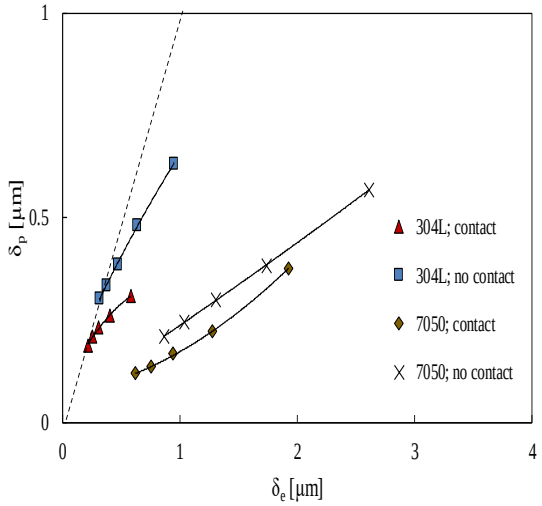

Figure 5.5. Plastic CTOD range, δ_p, versus elastic CTOD range, δ_e (plane stress).

Figure 5.6 (a) presents the stress-strain response obtained from a particular Gauss point placed at a distance of 1.184 mm from the initial crack tip position, as schematized in Figure 5.6 (c). Each crack increment corresponds to 8 μm, therefore 148 crack increments were performed. At the first load cycle, there is some plastic deformation, which indicates that the Gauss point belongs to the monotonic plastic zone ahead of the crack tip, but there is no reversed plastic deformation. The progressive approximation of the crack tip to the Gauss point increases the stress and strain levels there. The largest loops are obtained when the Gauss point is immediately ahead of the crack tip. The two load cycles applied between crack increments are now clearly visible. A major output from Figure 5.6 (a) is the complexity of the stress-strain evolution at a particular point.

Figure 5.6 (b) compares the final loops for E=196 GPa and E=245 GPa when the Gauss point is immediately ahead of the crack tip. The lines at the top define the plastic deformation. That plastic deformation is larger for the lower value of E. This trend was also observed at the first load cycle. The grey line represents the full stress-strain response observed for E=196 GPa, which can be compared with similar results for E=245 GPa presented in Figure 5.6 (a). The global variation is quite similar, but the values of plastic deformation are slightly different.

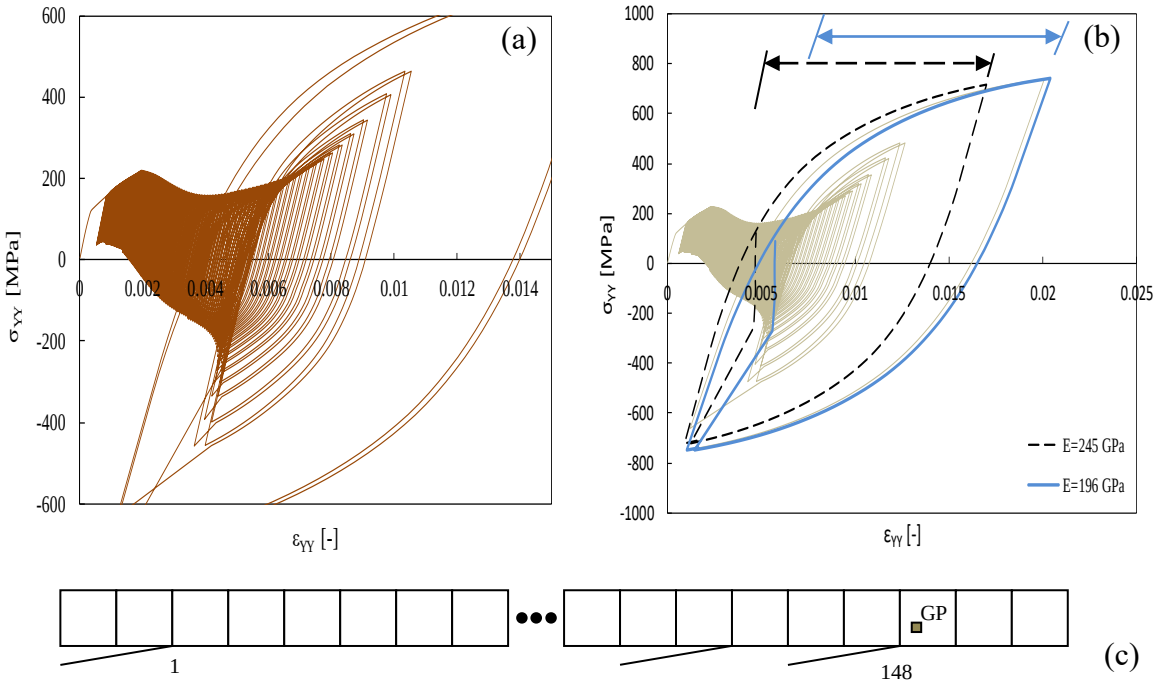

Figure 5.6. Stress-strain curves (a) E=245 GPa. (b) E=196 GPa, highlighting the effect of E on final loops (E=245 GPa and E=196 GPa). (c) Schematic representation of Gauss point, at a distance of 1.184 mm ahead of the initial crack tip position, and crack growth (SS304L; plane stress; no contact).

5.3. Effect of E with crack closure

Figure 5.7 (a) plots the CTOD versus the applied load for the SS304L assuming three values of Young's modulus (147 GPa, 196 GPa, and 245 GPa) which correspond, respectively, to the cases "0.75E", "Reference" and "1.25E" (see Table 4.1) with contact of crack flanks.

As it can be observed the decrease of Young´s modulus causes an increase of the CTOD. This was expected because, with the reduction of E, the material is more flexible. This effect is more prominent for higher loads. The crack opening and closure levels do not seem to be significantly affected. Figure 5.7 (b) plots the $CTOD_p$ versus the applied load. As can be seen, the increase in Young´s modulus causes a decrease in plastic CTOD. For relatively low loads the curves are almost coincident, and the separation occurs only for relatively high loads.

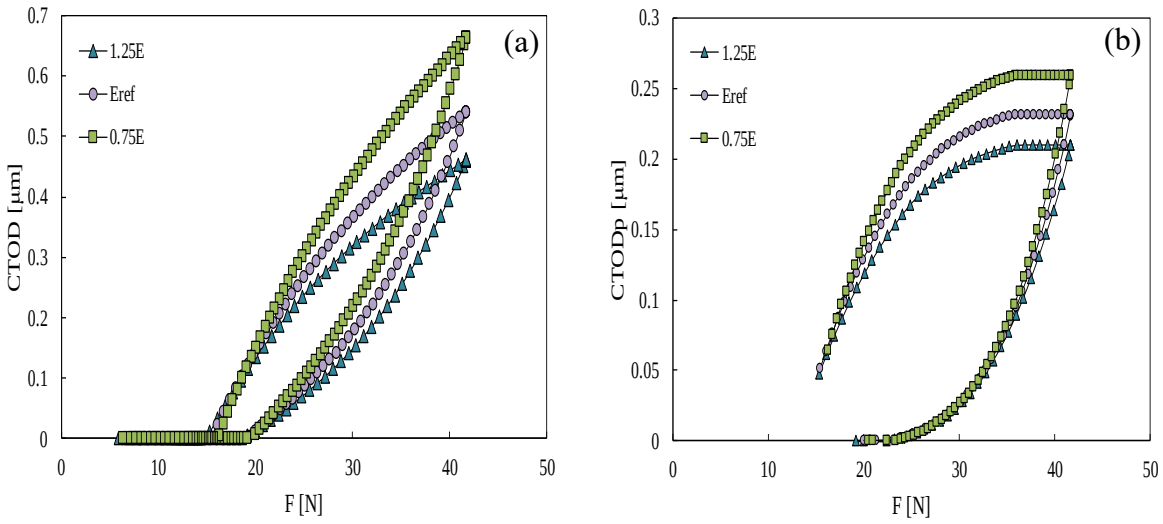

Figure 5.7. CTOD versus load; (b) plastic CTOD versus load (SS304L; plane stress; contact).

Figure 5.8 plots the plastic CTOD range (δ_p) versus 1/E, in plane stress state with contact of crack flanks. As it is shown, the increase of 1/E increase δ_p in all cases studied, i.e., the higher the E values, the lower the plastic CTOD range. Linear trendlines were added with good correlation coefficients. However, the correlation coefficients are worse than those obtained for the series without contact, which means that the phenomenon of crack closure introduces some non-linearity in the relation between δ_p and 1/E.

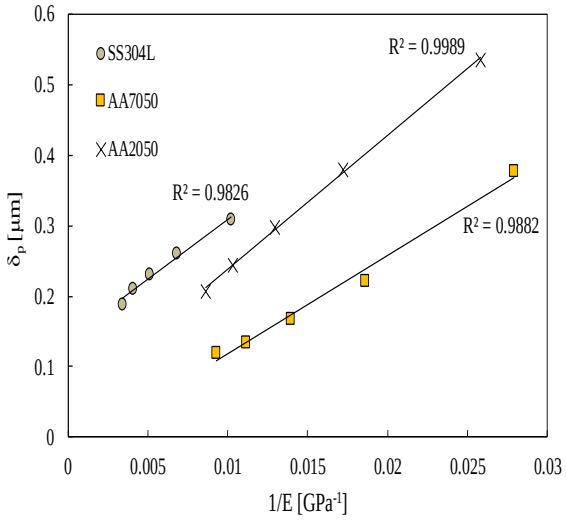

Figure 5.8. Plastic CTOD range, δ_p, versus the inverse of the Young´s modulus (Contact of crack flanks, plane stress).

Figure 5.9 plots $U_{closure}$ versus E for the cases with contact between crack flanks. $U_{closure}$ represents the portion of load cycle during which the crack is closed, and is given by:

$$U_{closure} = \frac{F_{open} - F_{min}}{F_{max} - F_{min}} \times 100, \tag{5.1}$$

where F_{open} is the crack opening load and F_{max} and F_{min} are the maximum and minimum loads in a loading cycle. There is a relatively small variation with Young's modulus, which was expected considering the results of Figure 5.3.

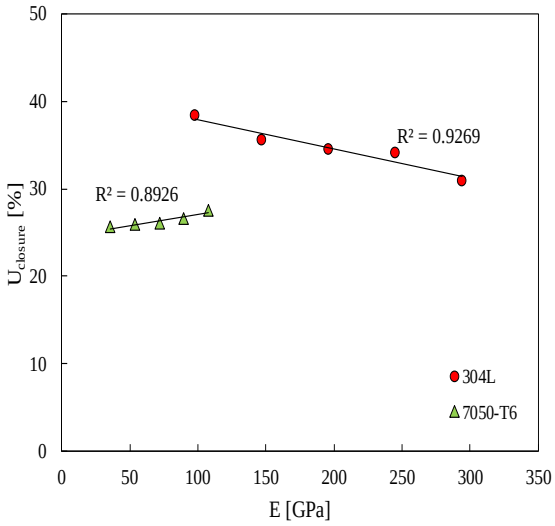

Figure 5.9. Crack closure versus Young´s Modulus (SS304L; plane stress and AA7050-T6; plane stress).

The values for the AA7050-T6 are in the range 25-30%, increasing with E. On the other hand, for the SS304L, the values are in the range 30-40%, decreasing with E.

Figure 5.10 shows the effect of crack closure on δ_p-1/E relationship. There is a significant reduction in δ_p, which increases with 1/E. In fact, as can be seen in Figure 5.1 (a), the phenomenon of crack closure reduces the effective load range, producing a reduction of the elastic and plastic deformations. Some non-linearity can be seen, which reduces the correlation coefficient.

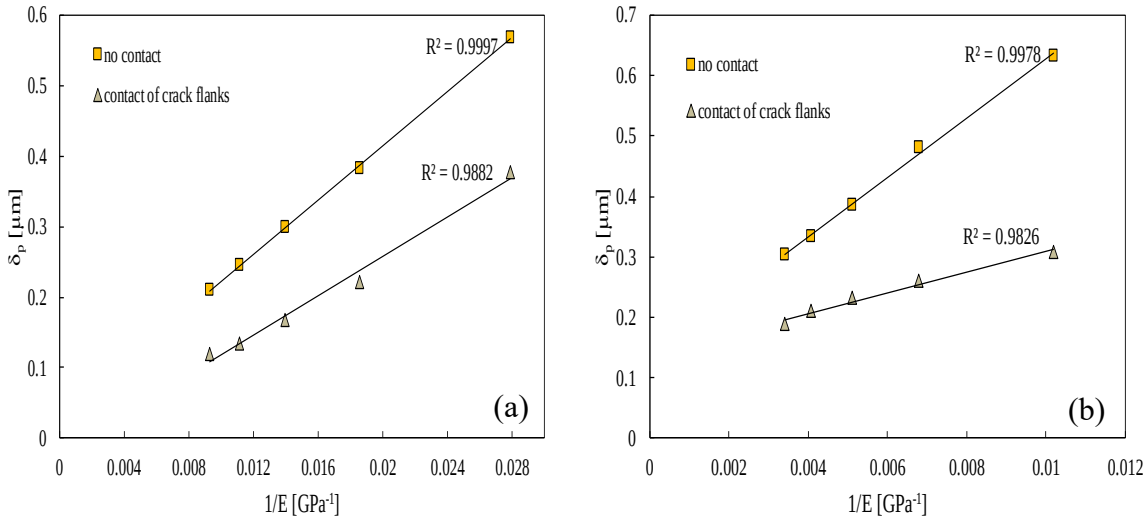

Figure 5.10. Effect of crack closure on δ_p versus 1E plots. (a) AA7050-T6; (b) SS304L.

5.4. Effect of Y_0 without crack closure

The contact between crack flanks can be avoided numerically, which is very interesting because it eliminates the crack closure phenomenon, as already mentioned. Therefore, the effect of material's yield stress can be studied singly. The AA7050-T6 has a pure kinematic behaviour, therefore the variation of Y_0 was accomplished by the variation of the isotropic saturation value (Y_{sat}). On the other hand, for the SS304L, only Y_0 was changed since the isotropic saturation value is always above Y_0, see Table 4.1.

Variations of the yield stress (cases "$0.75Y_0$", "Ref" and "$1.25Y_0$", see Table 4.1) were made to compare different curves of CTOD and plastic CTOD versus load in simulations without contact. The curves are shown in Figure 5.11 (a) and (b). From Figure 5.11 (a), as can be seen, the curves start apart and tend to approach for higher loads. The slope in the elastic regime is almost the same for the three situations. This is logical since

this regime is greatly dependent on Young's modulus, which is not changed. An increase of the yield stress causes the material to enter the plastic regime for higher values of load and less plastic CTOD range is achieved, as it is shown in Figure 5.11 (b). In other words, as expected, the elastic regime extends with the increase of material's yield stress. It was also found that these curves were almost overlapped for the SS304L.

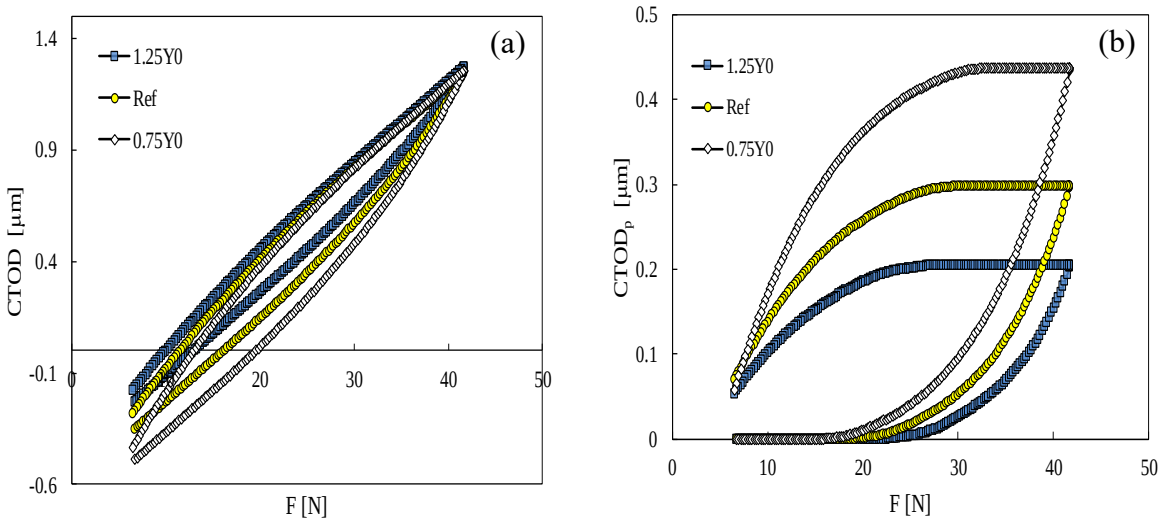

Figure 5.11 (a) CTOD versus load; (b) plastic CTOD versus load (AA7050-T6; plane stress; no contact).

Figure 5.12 presents the variation of plastic CTOD range with the yield stress, Y_0. In this picture, points located at 0% means that the yield stress assumes the reference value. The other four points correspond to more and less 25% and 50% of the elastic limit, as indicated in Table 4.1. It is observed a decrease in plastic CTOD with the increase of the yield stress, as could be expected. The decrease is more significant for AA7050-T6 than for the SS304L, and for this case is quite small. This indicates that the influence of Y_0 greatly depends on other material properties. Looking at Table 4.1, it is possible to see that the SS304L has a constant value of isotropic saturation stress, Y_{Sat}, therefore this parameter probably has a higher sensitivity in δ_p than Y_0.

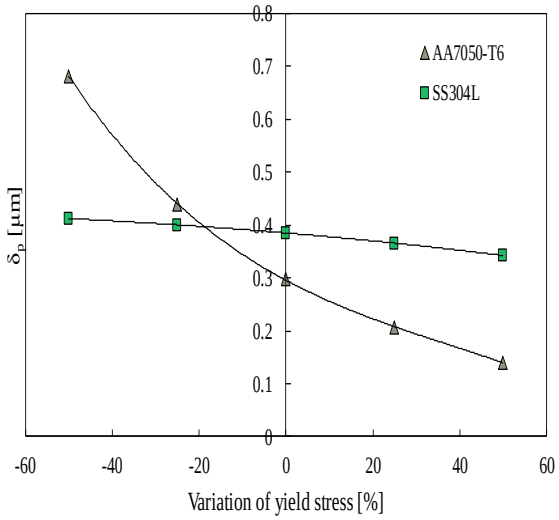

Figure 5.12. Plastic CTOD range, δ_p, versus the variation of the yield stress relative to the reference value in percentage.

Figure 5.13 shows stress-strain curves for a Gauss Point located at a distance of 1.184 mm from the initial crack tip position, for the reference value and a yield stress value 1.25 times superior, and it is also highlighted the final loops. The location of the Gauss Point and the successive positions of the tip are schematically shown in Figure 5.6 (c). Since the elements have dimensions 8×8 μm^2, 148 crack increments were performed.

As it is shown, the effect of the variation on the yield stress can be seen since the first cycle, where for a fixed value of plastic deformation, the increase of the elastic limit causes an increase of the stress required to achieve that value of deformation. The plastic deformation in the first cycle also indicates that the Gauss Point is inside the first monotonic plastic zone. As the crack propagation occurs, the range of stresses increases, causing more deformation. Compressive stresses increase in magnitude, beginning to produce inverse deformation. The largest values of stress happen when the Gauss Point is immediately ahead of the crack tip. From the final loops, it can be concluded that the reference curve has a bigger range of deformation than the $1.25Y_0$, as was expected.

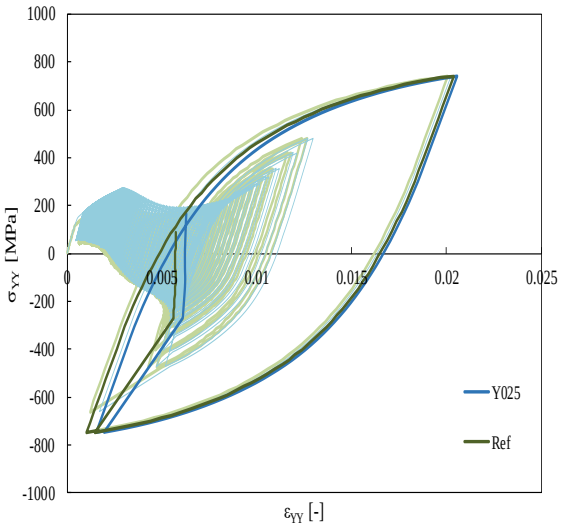

Figure 5.13. Stress-strain curves for the reference value of the yield stress and 1.25 times that value (SS304L, plane stress, no contact).

Figure 5.14 (a) and (b) plot load versus $CTOD_p$ for SS304L and AA7050, respectively, in plane stress conditions. The objective is to study the material hardening at the crack tip, as a function of the yield stress. Further increases in load are required to increase plastic CTOD. Also, the rate of variation of plastic CTOD increases with the decrease of the yield stress. The curves are nearly coincident for lower values of applied load in SS304L, which means that in these conditions, for a fixed value of the load, a variation in the yield stress practically does not change the plastic CTOD.

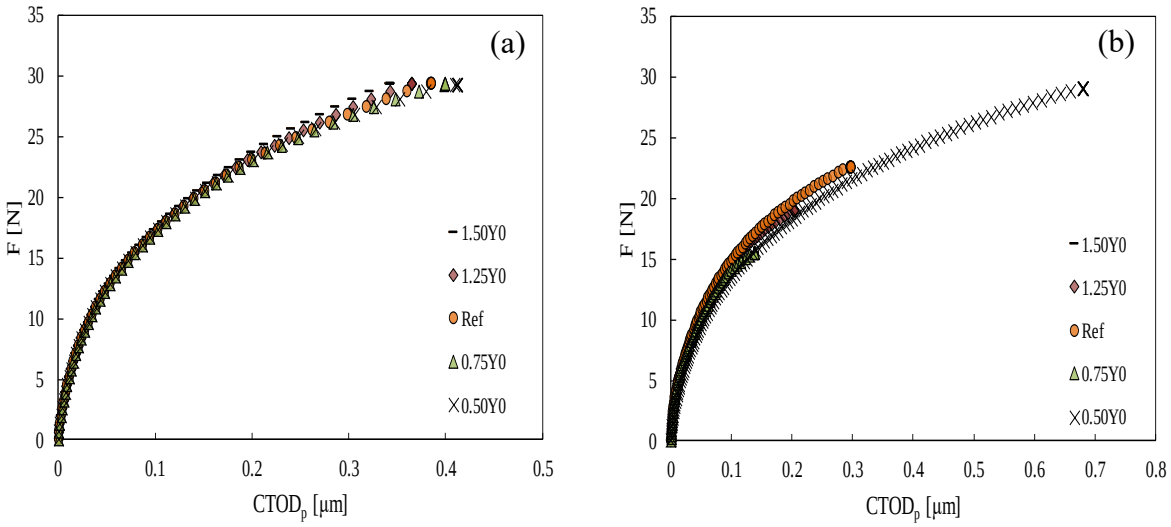

Figure 5.14. Load versus plastic CTOD. (a) SS304L; plane stress; (b) AA7050-T6; plane stress (without contact).

This is according to the results of Figure 5.12. The separation of the curves are more prominent for the AA7050 and this effect begins to be seen in lower values of applied loads.

To test the relations proposed in the literature, see Table B.1, a graph comparing δ_p with $1/Y_o$ is represented in Figure 5.15, where linear trendlines were added. A very good correlation coefficient was obtained for AA7050 In the case of SS304L, the correlation coefficient is worse, but as previously stated, the yield stress does not change much the plastic CTOD range in SS304L.

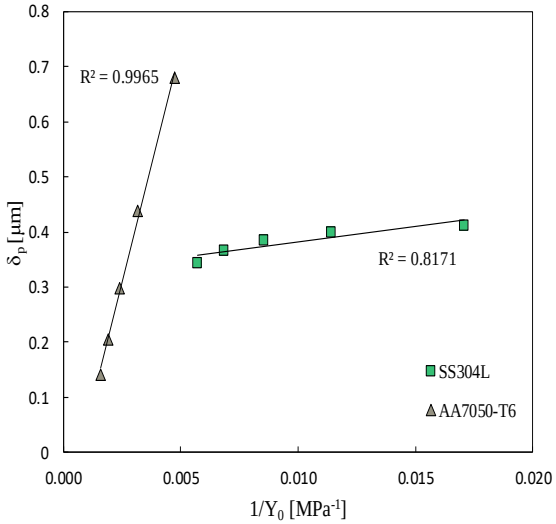

Figure 5.15. Plastic CTOD range, δ_p, versus the inverse of the yield stress (no contact; plane stress).

5.5. Effect of Y_0 with crack closure

Three curves of CTOD versus applied load were plotted in a graph shown in Figure 5.16 (a). Each curve corresponds to one value of initial yield stress which took the following values: 87.75 MPa, 117 MPa, and 146.25 MPa. As can be seen, the increase of yield stress for a constant load range causes a reduction of the CTOD, and higher crack opening and closure levels. The curves are almost overlapped for small values of the applied load. The separation of the curves occurs for relatively high values of load, when plastic deformation is notable, as shown in Figure 5.16 (b), that illustrates the plastic CTOD versus the applied load, for the same cases of the previous figure. It seems to have more discrepancy of the curves during unloading. Higher values of yield stress imply

larger elastic regime at the crack tip, which causes the tip to enter plastic deformation for higher loads.

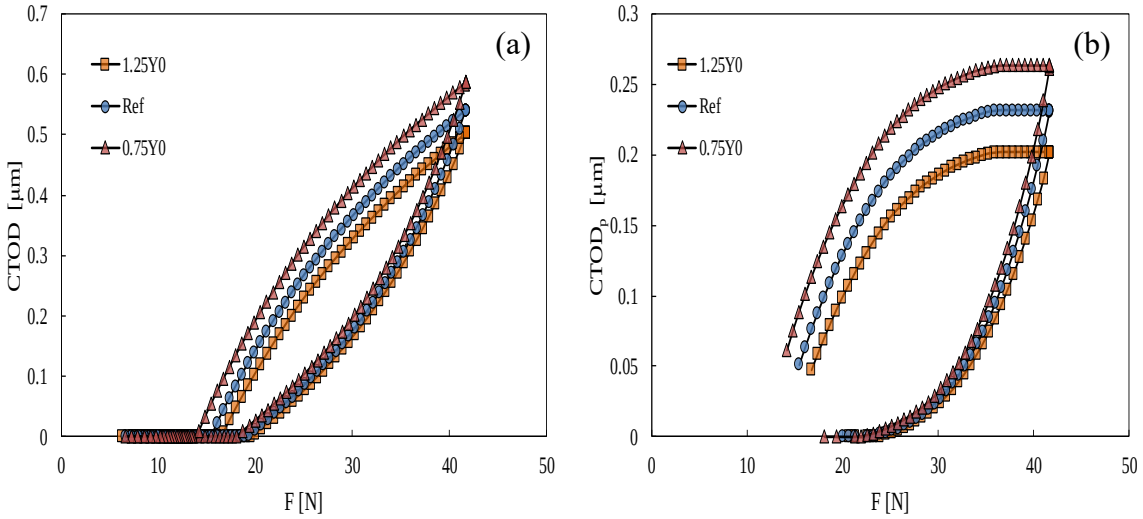

Figure 5.16. (a) CTOD versus load; (b) plastic CTOD versus load (AA7050-T6; plane stress; contact).

Figure 5.17 plots $U_{closure}$ versus the variation of the yield stress in percentage for the cases with contact between crack flanks. The yield stress has a great influence on the level of crack closure for the AA7050-T6. Increasing the elastic limit from -50% to 50% causes a 30% decrease in crack closure level. On the other hand, for the SS304L, an increase of the elastic limit from -50% to 50% causes an increase of 10% in crack closure level. Therefore, the crack closure level seems to be also more affected by Y_{Sat} than by Y_0.

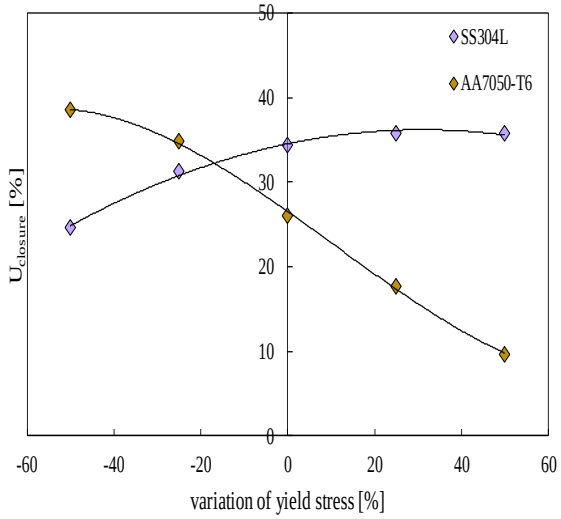

Figure 5.17. Crack closure versus the variation of the yield stress relative to the reference value in percentage (SS304L; plane stress and AA7050-T6; plane stress).

Figure 5.18 (a) and (b) plots δ_p versus the variation of the yield stress, without and with contact of crack flanks, respectively, in order to understand the effect of crack closure phenomenon. The first aspect is that crack closure has a great influence on δ_p, and therefore on FCG rate. For the AA7050-T6 the decrease of δ_p is much more evident for relatively low values of Y_0.

This is in accordance with Figure 5.17, which shows higher values of crack closure level for lower values of Y_0. At relatively high values of Y_0, Uclos≈10%, i.e., is relatively small, therefore there is a minor effect on δ_p. For the 304L stainless steel, the opposite trend is observed, i.e., the increase of Y_0 increases the influence of crack closure, which is also according to Figure 5.17.

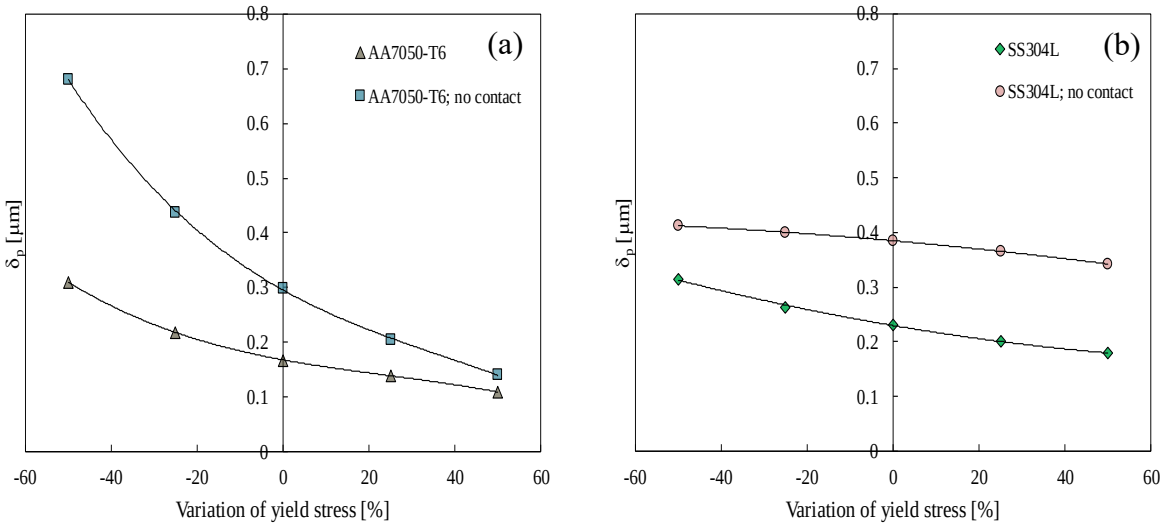

Figure 5.18. Plastic CTOD range, δ_p, versus the variation of the yield stress relative to the reference value in percentage (plane stress) (a) AA7050-T6; (b) SS304L.

Figure 5.19 (a) and (b) plots load versus $CTOD_p$ for SS304L and AA7050, respectively, in plane stress conditions. The objective is to study the material hardening at the crack tip, as a function of the yield stress. Further increases in load are required to maintain the increase in plastic CTOD. Also, the rate of variation of plastic CTOD increases with the decrease of the yield stress. The curves are nearly coincident for lower values of applied load in SS304L, which means that in these conditions, for a fixed value of the load, a variation in the yield stress practically does not change the plastic CTOD. The separation of the curves are more prominent in AA7050 and this effect begins to be seen in lower values of applied loads.

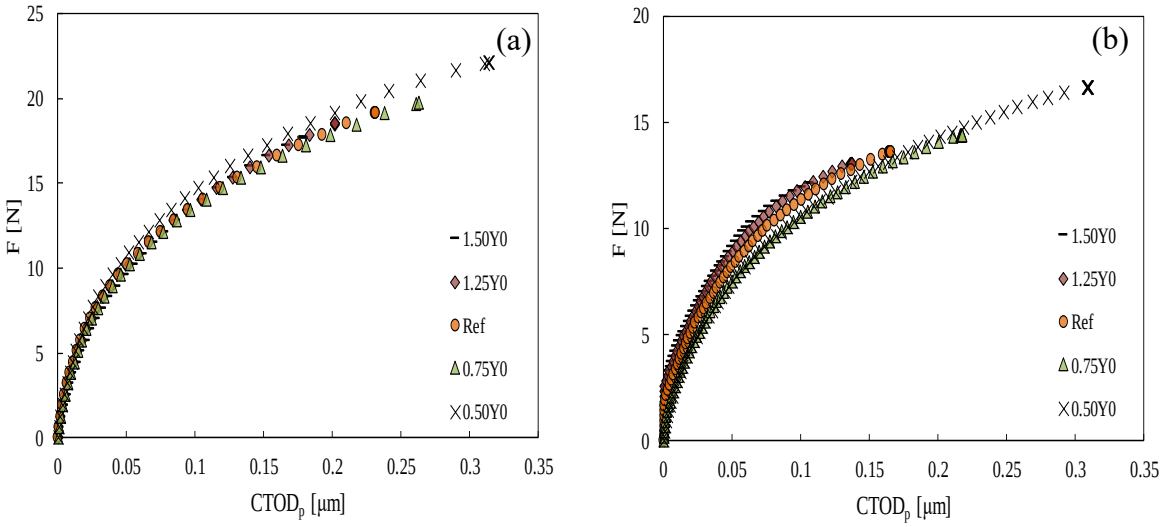

Figure 5.19. Load versus plastic CTOD. (a) 304L; plane stress contact; (b) AA7050-T6; plane stress with contact.

The models proposed in the literature (Table B.1) were are also tested in contact simulations as it is shown in Figure 5.20 that plots δ_p against $1/Y_o$. As in no contact simulation, the AA7050 shows a good relationship between δ_p and $1/Y_o$. However, for the SS304L, some nonlinearity is observed when the crack closure effect is present.

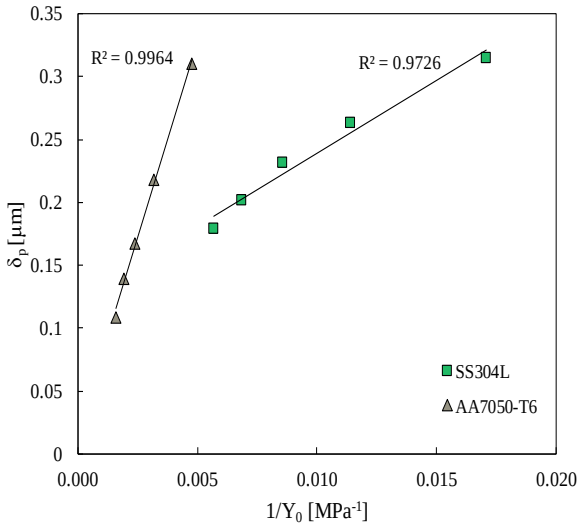

Figure 5.20. Plastic CTOD range, δ_p, versus the inverse of the yield stress (contact; plane stress).

5.6. Effect of X_{Sat} and C_X with crack closure

A pure kinematic hardening model was proposed for SS304L, to compare the results obtained with the mixed (isotropic and kinematic) hardening. The same conditions (specimen, loading, stress state, mesh, etc.) were employed in these simulations. Only simulations with contact at the crack flanks were performed. The objective was to elaborate a parametric analysis in X_{Sat} and C_X and compare the results in δ_p and $U_{closure}$.

The numerical simulations were performed in DD3IMP with the only difference occurring in the mater1.dat file. The isotropic saturation stress (Y_{Sat}) was equalised with the yield stress (Y_0). That is, Y_{Sat} took the value of 117 MPa instead of 204 MPa as it was identified in 1.

Figure 5.21 (a) compares the CTOD versus load curves, for the reference cases, between mixed and kinematic hardening. The opening displacement of the tip is higher in kinematic hardening. Also, the crack opens for lower values of load in kinematic hardening. Higher values of plastic CTOD are achieved in kinematic hardening, as schematized in Figure 5.21 (b). The differences in ranges, between mixed and kinematic, in plastic CTOD and in CTOD are practically the same meaning that the elastic regime was not affected by the changes made, as was expected.

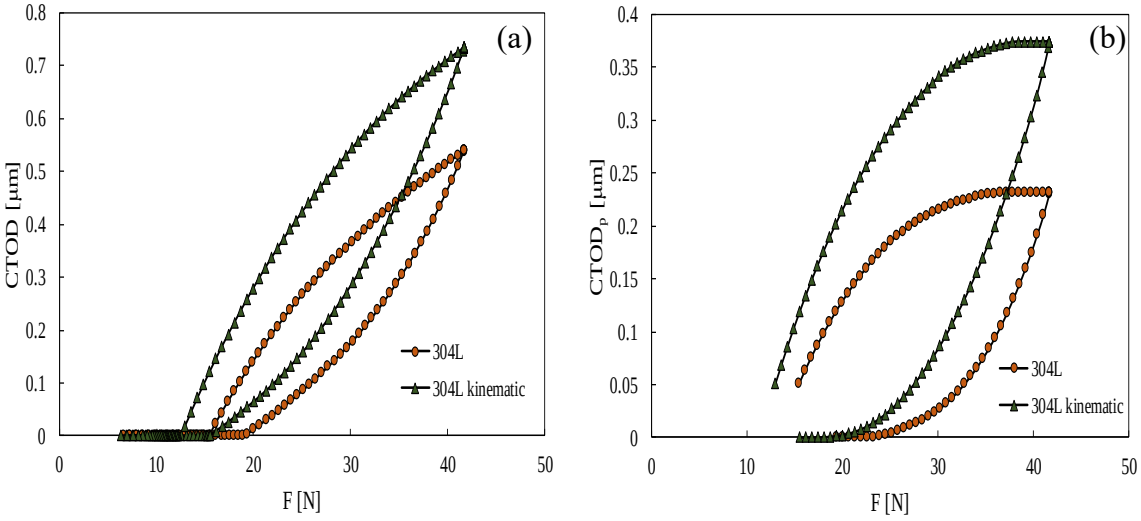

Figure 5.21. Effect of kinematic hardening in reference properties (SS304L, contact, plane stress). (a) CTOD versus F; (b) $CTOD_p$ versus F.

The variation in δ_p by changing X_{Sat} is shown in Figure 5.22 (a). In both kinematic hardening and mixed hardening, the increase of X_{Sat} causes a non-linear decrease of δ_p. This decrease is more prominent for the kinematic hardening.

In Figure 5.22 (b) $U_{closure}$ is plotted versus X_{Sat} and there is an increase of crack closure level with the increase of kinematic saturation stress, which explains the decrease of δ_p observed in Figure 5.22 (a). Also, $U_{closure}$ is lower in kinematic hardening.

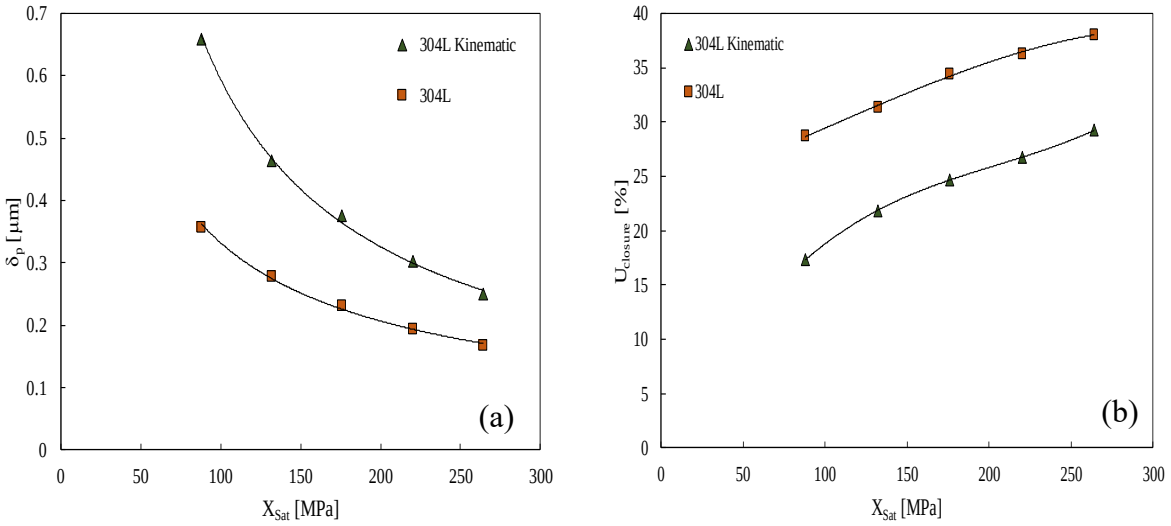

Figure 5.22. Comparison between 304L pure kinematic hardening and 304L mixed hardening (contact, plane stress). (a) δ_p versus X_{Sat}; (b) $U_{closure}$ versus X_{Sat}.

A decrease of δ_p is also observed when C_X is increased for both mixed (isotropic and kinematic) hardening and kinematic hardening, as it is shown in Figure 5.23 (a) that plots δ_p against C_X. More plastic deformation ranges are achieved in the kinematic hardening.

A comparison of crack closure level with C_X is presented in Figure 5.23 (b). As in Figure 5.22 (b), the kinematic hardening has lower crack closure levels than mixed hardening but in opposition to Figure 5.22 (b), C_X does not seem to influence $U_{closure}$ like X_{Sat}.

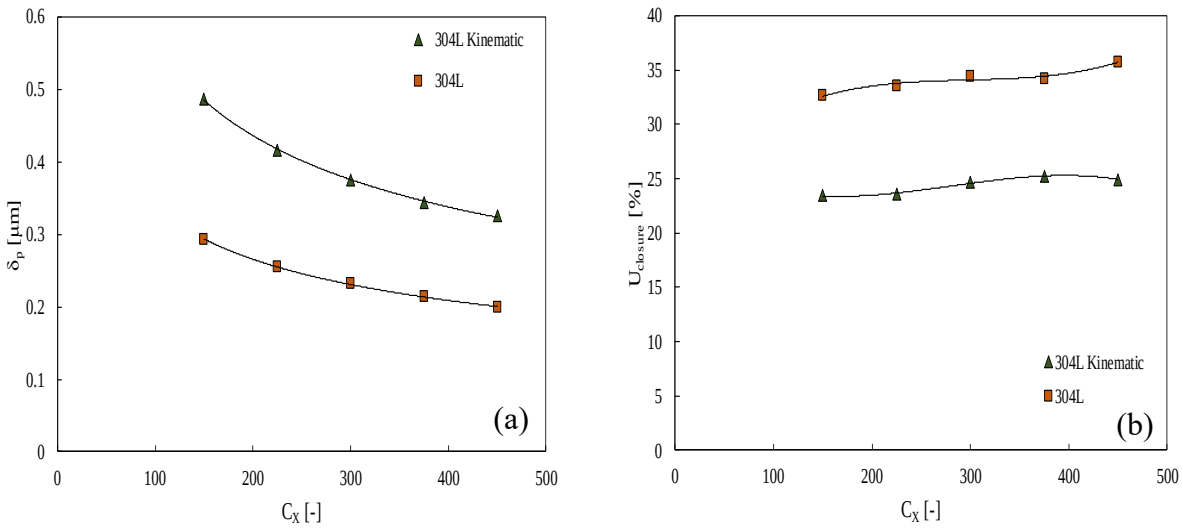

Figure 5.23. Comparison between 304L pure kinematic hardening and 304L mixed hardening (contact, plane stress). (a) δ_p versus C_X; (b) $U_{closure}$ versus C_X.

The final loops of stress-strain curves plotted for the reference properties and calculated at the GaussPoint indicated in Figure 5.6 (c), are represented in Figure 5.24. As can be seen, the kinematic hardening causes more cyclic plastic zone due to the characteristic softening observed in this type of hardening, which explains the lower crack closure level observed in kinematic hardening curves in Figure 5.22 (b) and Figure 5.23 (b).

In addition, less $U_{closure}$ causes more effective load, therefore more plastic deformation is achieved, as indicated in Figure 5.22 (a) and Figure 5.23 (a).

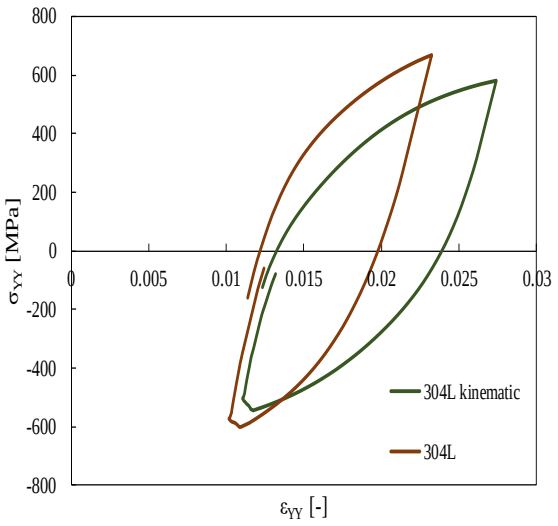

Figure 5.24. Final loops of stress-strain curves for the reference properties (SS304L, plane stress, contact).

Also, by looking at Figure 5.25 (a) and (b) that show the final loops of stress-strain curves for 304L kinematic, it is seen that the increase of both X_{Sat} and C_X causes less deformation. This can be explained by the activation of multiple slips, which cause interaction between dislocations functioning as barriers to the dislocation motion, causing less deformation, mainly plastic deformation.

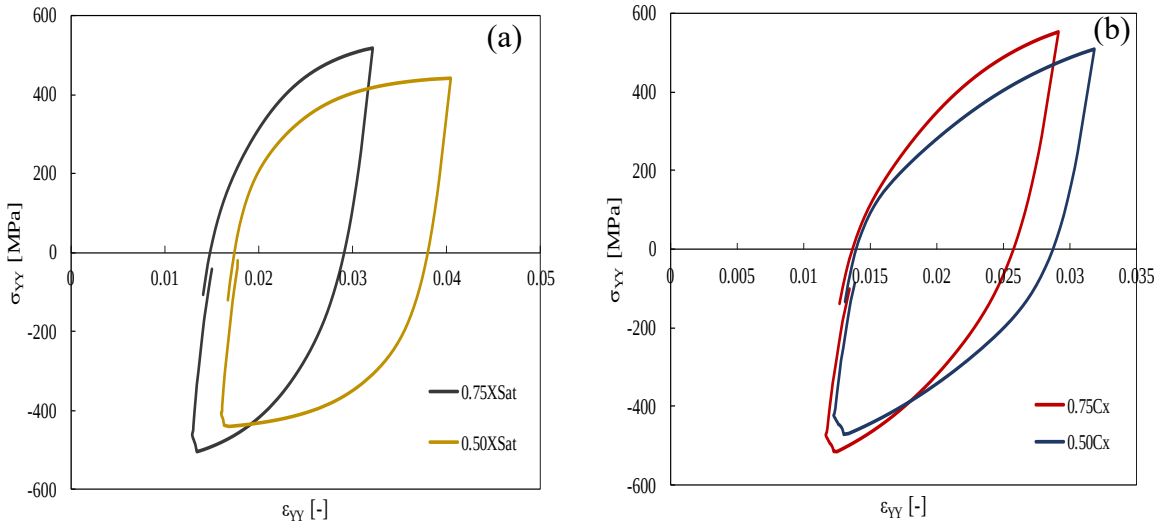

Figure 5.25. Final loops of stress-strain curves (SS304L kinematic, plane stress, contact). (a) 0.50 X_{Sat} and 0.75 X_{Sat}; (b) 0.50 C_X and 0.75 C_X.

Figure 5.26 (a) and (b) intend to show the hardening at the crack tip by plotting load versus plastic CTOD, for both mixed and kinematic hardening, by varying X_{Sat} and C_X respectively. The plastic CTOD rate increases with the decrease of X_{Sat} and C_X, and also in kinematic hardening simulations. Higher values of load are required when the kinematic properties increase and in mixed hardening simulations, becoming it is more difficult to plastically deform and by consequence more difficult to occur crack propagation.

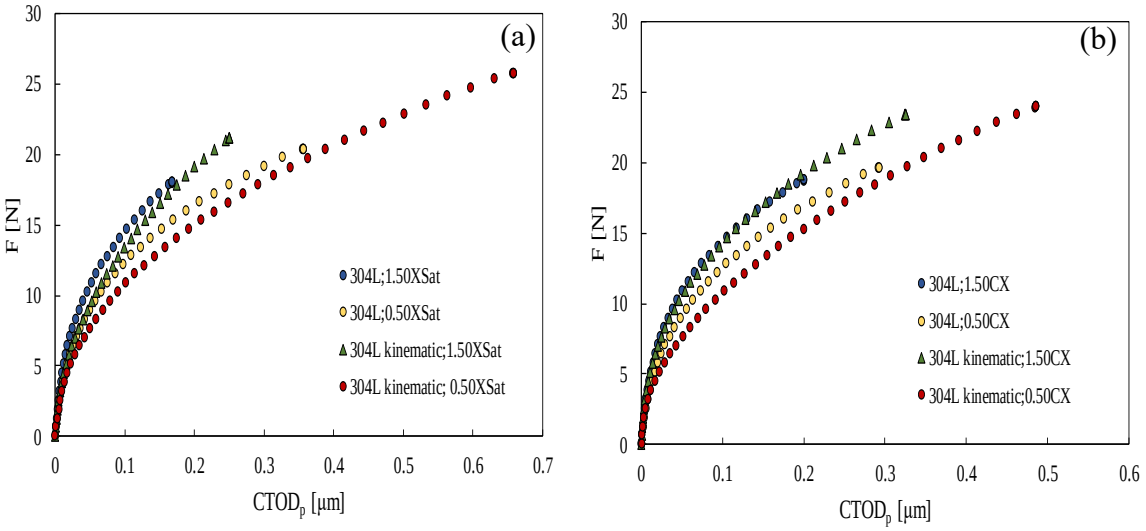

Figure 5.26. Load versus plastic CTOD for SS304L mixed and kinematic hardening (contact, plane stress). (a) 0.50 and 1.50 X_{Sat}; (b) 0.50 and 1.50 C_X.

5.7. Effect of Y_{Sat} and C_Y with crack closure

The objective in this section was to study the effect of Y_{Sat} and C_Y in simulations with crack closure, by comparing mixed (isotropic and kinematic) hardening and pure isotropic hardening. Due to the lack of time pure isotropic hardening was not studied. As such, only mixed hardening results will be presented.

Three curves of CTOD versus F, corresponding to the cases "1.25 Y_{Sat}", "0.75 Y_{Sat}" and "Reference" were plotted to study the changes in these curves by changing the isotropic saturation stresses values. Higher values of saturation stress cause the material to have more difficulty to plastically deform, due to multiple slips interfering with each other, preventing the crack to open more easily, as can be seen by the crack opening loads and by the CTOD ranges. The difference in CTOD and plastic CTOD ranges are practically the same, meaning that the elastic CTOD ranges are not affected by changing the isotropic saturation stress.

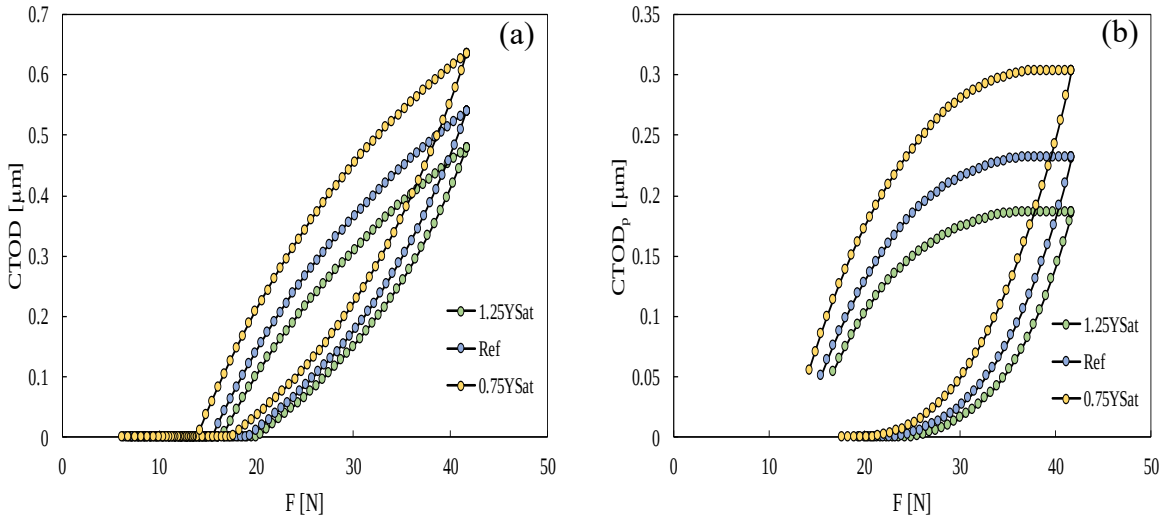

Figure 5.27. (a) CTOD versus F; (b) $CTOD_p$ versus F. 304L mixed hardening (contact, plane stress).

Such as for kinematic saturation stress, the increase of isotropic saturation stress causes the decrease of plastic CTOD range and an increase of crack closure level, as it is shown in Figure 5.28 (a) and (b), respectively. The same is observed about C_Y, however, there are fewer variations of plastic CTOD range, Figure 5.29 (a), and crack closure level, Figure 5.29 (b), which indicates that C_Y probably has less sensitivity in δ_p than Y_{Sat}.

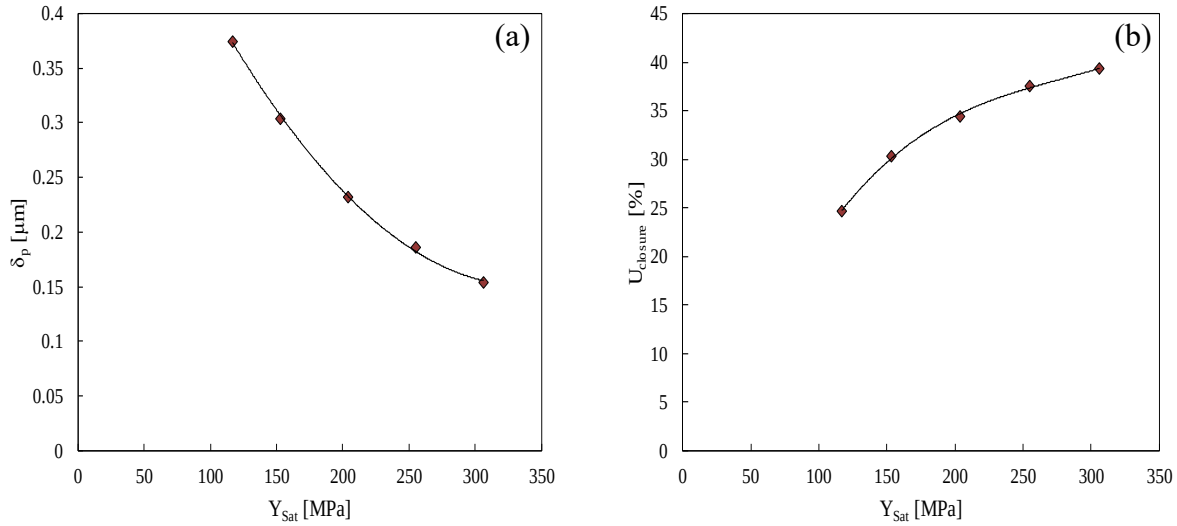

Figure 5.28. (a) δ_p versus X_{Sat}; (b) $U_{closure}$ versus X_{Sat}. 304L mixed hardening (contact, plane stress).

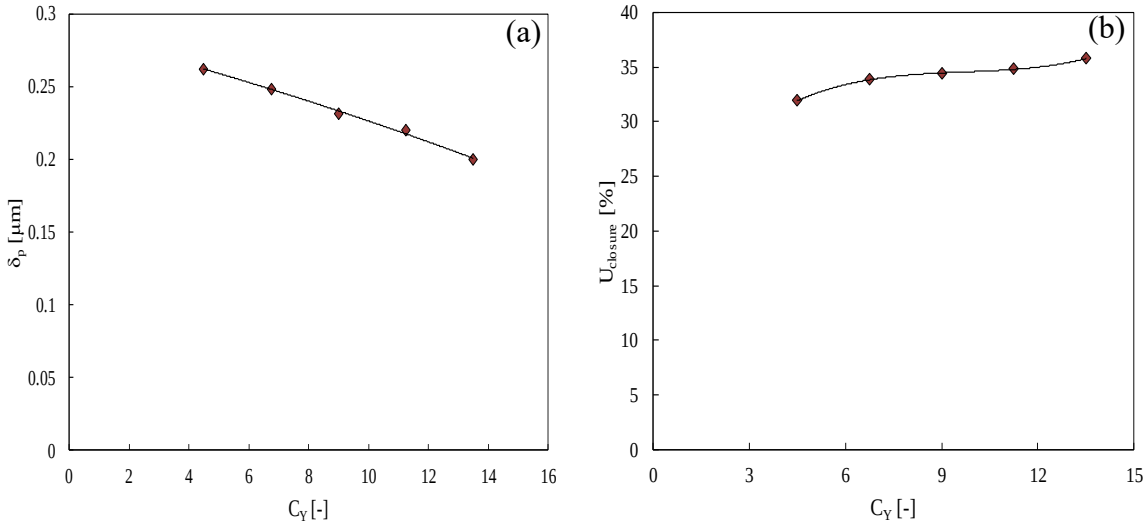

Figure 5.29. (a) δ_p versus C_Y; (b) $U_{closure}$ versus C_Y. 304L mixed hardening (contact, plane stress).

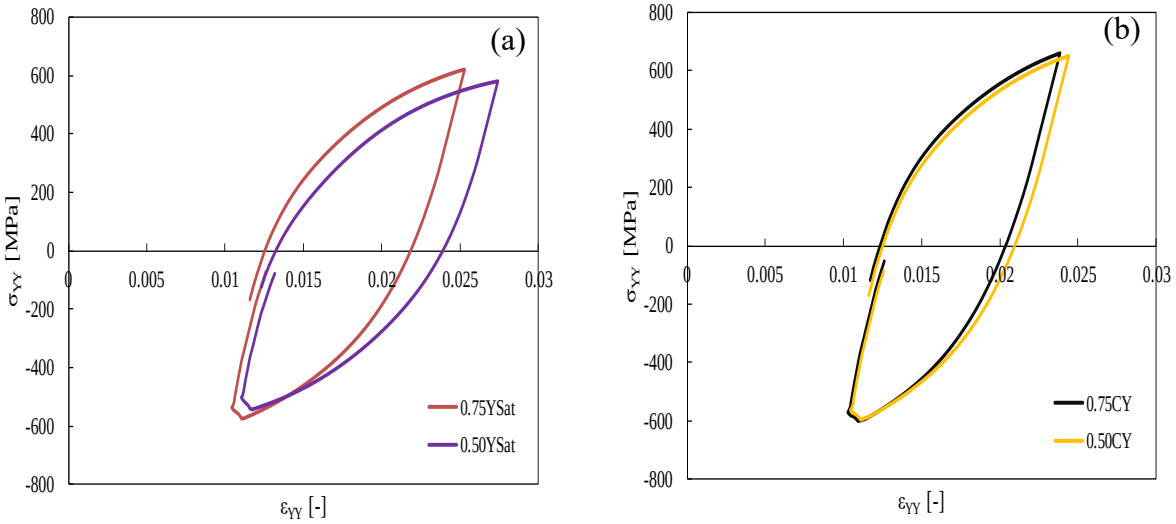

Figure 5.30. Final loops of stress-strain curves (SS304L, plane stress, contact). (a) 0.50 Y_{Sat} and 0.75 Y_{Sat}; (b) 0.50 C_Y and 0.75 C_Y.

Figure 5.30 (a) and (b) shows the final stress-strain loops by changing Y_{Sat} and C_Y, respectively. The increase in these properties causes more dislocation motion, which will produce more interferences, making it more difficult for the material to deform.

Even though the pure isotropic hardening was not modelled, it is expected that lower values of plastic CTOD range can be achieved, as well as less cyclic plastic zone in the final loops, because in this type of hardening there is less ability for the material to soften, in comparison with the kinematic hardening, during the cyclic loading.

The hardening at the crack tip is represented in Figure 5.31 (a) and (b) and it was performed for the cases "0.50Y_{Sat}", "1.50Y_{Sat}", "0.50C_Y" and "1.50C_Y". A continuous increase in load is required for the plastic CTOD to increase. The rate of plastic CTOD is higher when Y_{Sat} and C_Y decrease. There is a greater difference between the curves in cases where it was varied C_Y.

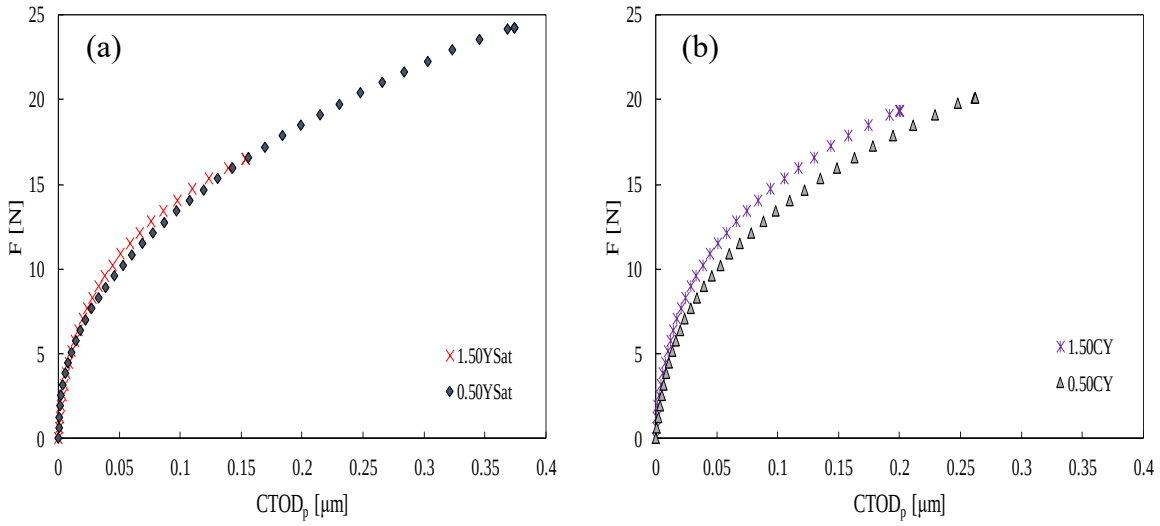

Figure 5.31. Load versus plastic CTOD for SS304L mixed hardening (contact, plane stress). (a) 0.50 and 1.50 Y_{Sat}; (b) 0.50 and 1.50 C_Y.

6. DISCUSSION

6.1. Sensitivity Analysis

A sensitivity analysis was developed to quantify the relative importance of the different material parameters. Local sensitivity analysis aims at estimating the influence of the input parameters on the output quantities in one particular point of the input parameter space [52]. The non-dimensional sensitivity of δ_p to the different material parameters is expressed as follows:

$$\nabla f = \frac{\partial \delta_p}{\partial m_p} \cdot \frac{m_p}{\delta_p}. \tag{6.1}$$

where ∇f is the sensitivity coefficient and m_p represents the material parameter. The elasto-plastic properties studied regarding the variation of plastic CTOD were: Young´s modulus (E), kinematic hardening parameters (C_X and X_{Sat}), and isotropic hardening parameters (Y_0, $Y_{Sat,}$ and C_Y). Each sensitivity coefficient represents the change rate of the plastic CTOD range caused by a variation of a specific material parameter. Note that a sensitivity of 0.5 indicates that a variation of 1% in m_p produces a variation of 0.5% in δ_p.

All sensitivity calculations were aimed at specific reference points. A change in the calculation point causes deviations in the values of sensitivity obtained.

6.1.1. Sensitivity analysis without crack closure

In Figure 6.1 (a) is shown the non-dimensional sensitivity of δ_p to the different material parameters, for SS304L. As can be seen, the most relevant parameter is the isotropic saturation stress (Y_{Sat}), as was previously predicted, followed by the kinematic saturation stress (X_{Sat}), the Armstrong -Frederick parameter (C_X) and the Young´s modulus (E). The plastic CTOD range has a very little sensitivity to C_Y and Y_0.

The same procedure was done for AA7050 as it is represented in Figure 6.1 (b). The yield stress is now the most important parameter, while X_{Sat} and C_X have minor influences than in the case of SS304L. Mean values of sensitivity were observed for E.

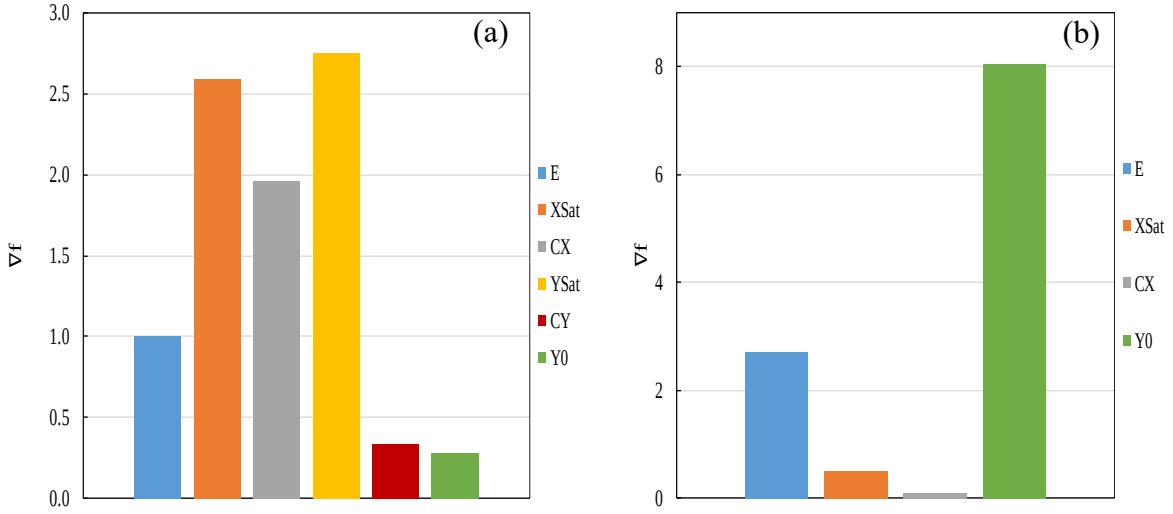

Figure 6.1. Sensitivity, ∇f, of the plastic CTOD range to the material parameters (plane stress; no contact). (a) SS304L; (b) AA7050-T6.

6.1.2. Sensitivity analysis with crack closure

Figure 6.2 (a) shows the sensitivity of δ_p to the elasto-plastic properties of SS304L. Y_0 is the most sensitive parameter followed by X_{Sat}, E, C_X, Y_{Sat}, and finally C_Y.

Comparing the cases of contact and no contact, there is a decrease in sensitivity of X_{Sat}, Y_{Sat}, and C_X, and a great increase of Y_0 in simulations with crack closure. The parameter C_Y seems to maintain the sensitivity. On the contrary, E is more relevant in simulations with contact at the crack flanks.

Comparing Figure 6.1 (b) with Figure 6.2 (b), there is an increase of the relevance of the parameters E, X_{Sat}, and C_X in simulations with crack closure effect in AA7050-T6. In contrast, it is found that the yield stress becomes the parameter less relevant.

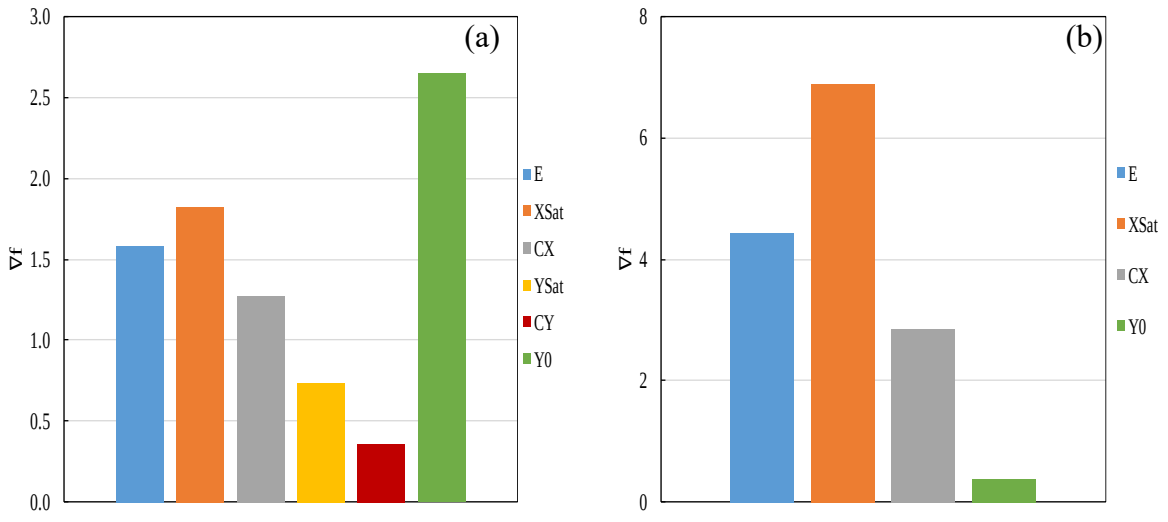

Figure 6.2. Sensitivity, ∇f, of the plastic CTOD range to the material parameters (plane stress; contact). (a) SS304L; (b) AA7050-T6.

From the review of the sensitivity analysis figures, the Young´s modulus, although it is an elastic parameter, has a relatively high influence on plastic CTOD range and therefore cannot be neglected. Also, the insertion of crack closure phenomenon can cause the yield stress to be the most relevant (SS304L, in simulations with contact, and AA7050-T6, in simulations without contact) or the less relevant parameter (SS304L, in simulations without contact, and AA7050-T6, in simulations with contact) in plastic CTOD range. The reduction of sensitivity to Y_0 is accompanied by an increase of sensitivity to the kinematic parameters with the exception of C_Y, and vice-versa.

7. CONCLUSIONS

In this thesis, it was performed a parametric study to understand the effect of elasto-plastic properties on FCG. The geometry, loading and material state were kept so that the results were not interfered by these changes.

Regarding the effect of Young's modulus (E):

- It is confirmed that the plastic CTOD range, δ_p, is proportional to the inverse of E, going towards most of the models proposed in the literature. This agreement reinforces the capability of da/dN versus plastic CTOD approach to predict the effect of different parameters on FCG.
- The insertion of crack closure phenomenon introduces some non-linearity between δ_p and $1/E$, reducing the correlation coefficients.
- The increase of Young's modulus causes more crack closure level in the AA7050-T6 and less in the SS304L, being this effect more prominent in the SS304L.

In relation to the effect of the yield stress (Y_0):

- Most solutions proposed in the literature point to a linear relation between δ_p and $1/Y_0$. This relation is proved to be true for the AA7050-T6 with excellent correlation coefficients in both contact and no contact simulations. However, some non-linearity was observed for the SS304L especially in contact simulations.
- The effect of Y_0 is found to be much more relevant for the 7050 aluminium alloy than for the 304L stainless steel, which indicates a major influence of other material properties, namely the isotropic saturation stress.
- With the inclusion of crack closure, the reduction of δ_p with Y_0 is kept, but there is a substantial reduction of δ_p and therefore of FCG rate.

In relation to the kinematic hardening parameters (X_{Sat} and C_X), performed for the SS304L in contact simulations:

- The increase of the kinematic saturation stress, X_{Sat}, is found to decrease, non-linearly, the plastic CTOD range in both pure kinematic hardening model and mixed (isotropic+kinematic) hardening model. This reduction is more pronounced in the pure kinematic model. In addition, the increase of this parameter causes the increase of crack closure level.
- A decrease in δ_p is observed with higher values of $C_{X,}$ in both models, however, the crack closure level suffers small variations.

Regarding the effect of isotropic hardening parameters (Y_{Sat} and C_Y):

- When the isotropic saturation stress, Y_{Sat}, increases, the plastic CTOD range decreases, non-linearly, and crack closure level increases.
- The same was observed for C_Y but with fewer variations.

The sensitivity analysis performed indicates that:

- The Young's modulus has a relatively high influence on plastic CTOD range, therefore the effect of this parameter on FCG cannot be neglected.
- The yield stress can be the most relevant parameter on δ_p, for the cases of AA7050-T6 without contact at the crack flanks and SS304L with contact, or the less relevant, for the cases of AA7050-T6 in contact simulations and SS304L without contact.
- It is observed that when the yield stress is the parameter less relevant, the saturation stresses assume higher values of relevance on δ_p.

As a final conclusion, for high fatigue strength, the material must have high Young's modulus (E) to increase stiffness, high yield stress (Y_0) to increase the elastic regime, and high values of saturation stresses (Y_{Sat} and X_{Sat}) and parameters (C_X and C_Y) to reduce the ability to plastically deform .

From this work three journal papers were produced. The front pages of these papers can be found in Annex A. Two of the papers were already accepted for publication, while the third one, focused on the effect of Young's modulus, is in the final revision for submission.

For future works, it is proposed:

- complete and submit the paper focused on the effect of Young's modulus;
- write a paper focused on the effect of kinematic hardening parameters. This paper will also include results without contact of crack flanks.
- write a paper focused on the effect of isotropic hardening parameters. This paper will also include results without contact of crack flanks.
- develop an empirical model for FCG based on the results obtained here. This will include a non-dimensional analysis.
- link the microstructure with the elastic-plastic properties. This is fundamental for the development of new alloys with improved fatigue properties.

BIBLIOGRAPHY

[1] K. Samadian, S. Hertelé, and W. De Waele, 'Measurement of CTOD along a surface crack by means of digital image correlation', *Eng. Fract. Mech.*, vol. 205, pp. 470–485, Jan. 2019.

[2] Q. Xin, *Diesel engine system design*. Woodhead Publishing, 2011.

[3] P. Paris and F. Erdogan, 'A Critical Analysis of Crack Propagation Laws', *J. Basic Eng.*, vol. 85, no. 4, p. 528, 1963.

[4] F. Erdogan and M. Ratwani, 'Fatigue and fracture of cylindrical shells containing a circumferential crack', *Int. J. Fract. Mech.*, vol. 6, no. 4, pp. 379–392, 1970.

[5] Hartman A and Schijve J, 'The effects of environment and load frequency on the crack propagation law for macro fatigue crack growth in aluminium alloys', *Eng. Fract. Mech.*, vol. 1, no. 4, pp. 615–631, 1970.

[6] Southwest Research Institute and NASA Johnson Space Center, 'NASGRO, Fracture mechanics and Fatigue Crack Growth Analysis Software (version 7.0)'. 2012.

[7] F. V. Antunes, S. M. Rodrigues, R. Branco, and D. Camas, 'A numerical analysis of CTOD in constant amplitude fatigue crack growth', *Theor. Appl. Fract. Mech.*, vol. 85, no. Part A, pp. 45–55, 2016.

[8] ASTM E647, 'Standard test method for measurements of fatigue crack growth rates", Annual Book of ASTM Standards', *Am. Soc. Test. Mater.*, vol. 03.01, pp. 578–614, 1995.

[9] C. Branco, J. Ferreira, J. Costa, and A. Ribeiro, *Projecto de Órgãos de Máquinas*. 2012.

[10] G. R. Irwin, 'Elasticity and Plasticity', in *Elasticity and Plasticity*, vol. 3, no. 6, Springer, Berlin, Heidelberg, 1958, pp. 551–590.

[11] T. L. Anderson, *Fracture Mechanics. Fundamentals and Applications*, 2nd ed. 1995.

[12] J. R. Rice, 'Mechanics of Crack Tip Deformation and Extension by Fatigue', *Fatigue Crack Propag.*, no. January 1967, p. 247, 1967.

[13] L. P. Borrego, J. M. Costa, F. V. Antunes, and J. M. Ferreira, 'Fatigue Crack Growth in Aluminium Alloys', PhD Thesis, Technology University of Delft, 2008.

[14] P. Paris, M. Gomez, and W. Anderson, 'A Rational Theory of Fatigue', *Trend Eng.*, vol. 13, pp. 9–14, 1961.

[15] F. V. Antunes, S. Serrano, R. Branco, and P. Prates, 'Fatigue crack growth in the 2050-T8 aluminium alloy', *Int. J. Fatigue*, vol. 115, no. September 2017, pp. 79–88, 2018.

[16] W. Elber, 'Fatigue crack closure under cyclic tension', *Eng. Fract. Mech.*, vol. 2, no. 1, pp. 37–45, 1970.

[17] L. Correia, 'Previsão da Vida de Propagação à Fadiga', PhD Thesis, Department of Mechanical Engineering, University of Coimbra, 2018.

[18] R. O. Ritchie, S. Suresh, and C. M. Moss, 'Near-Threshold Fatigue Crack Growth in 2 1/4 Cr-1Mo Pressure Vessel Steel in Air and Hydrogen', *J. Eng. Mater. Technol.*, vol. 102, no. 3, p. 293, 1980.

[19] S. Suresh and R. O. Ritchie, 'On the influence of fatigue underloads on cyclic crack growth at low stress intensities', *Mater. Sci. Eng.*, vol. 51, no. 1, pp. 61–69, 1981.

[20] S. Suresh and R. O. Ritchie, 'A geometric model for fatigue crack closure induced by fracture surface roughness', *Metall. Trans. A*, vol. 13, no. 9, pp. 1627–1631, 1982.

[21] R. Hosseini and R. Seifi, 'Influence of Hardening on the Cyclic Plastic Zone Around Crack Tip in Pure Copper CT Specimens', *J. Stress Anal.*, vol. 2, no. 2, pp. 2588–2597, 2018.

[22] A. A. Wells, 'Unstable Crack Propagation in metals, Cleavage and Fast Fracture', *Crack Propag. Symp. Cranf.*, vol. 1, no. 84, pp. 210–230, 1961.

[23] S. S. Committee, 'Elastic - Plastic Fracture Mechanics A Critical Review', 1990.

[24] X.-K. Zhu, P. Zelenak, and T. McGaughy, 'Comparative study of CTOD-resistance curve test methods for SENT specimens', *Eng. Fract. Mech.*, vol. 172, pp. 17–38, Mar. 2017.

[25] R. M. Pelloux, 'Crack Extension by alternating shear', *Eng. Fract. Mech.*, vol. 1, pp. 170–174, 1970.

[26] R. C. Bathes and SanthanamT., 'Relationship between notch tip strain and crack-opening displacement', *Mater. Sci. Eng.*, vol. 46, pp. 159–165, 1980.

[27] D. J. Nicholls, ‘The relation between crack blunting and fatigue crack growth rates’, *Fatigue Fract. Eng. Mater. Struct.*, vol. 17, no. 4, pp. 459–467, 1994.

[28] V. Tvergaard, ‘On fatigue crack growth in ductile materials by crack–tip blunting’, *J. Mech. Phys. Solids*, vol. 52, pp. 2149–2166, 2004.

[29] R. Pippan and W. Grosinger, ‘Fatigue crack closure: From LCF to small scale yielding’, *Int. J. Fatigue*, vol. 46, pp. 41–48, 2013.

[30] F. V. Antunes, R. Branco, P. A. Prates, and L. Borrego, ‘Fatigue crack growth modelling based on CTOD for the 7050-T6 alloy’, *Fatigue Fract. Eng. Mater. Struct.*, vol. 40, no. 8, pp. 1309–1320, 2017.

[31] F. V. Antunes, M. S. C. Ferreira, R. Branco, P. Prates, C. Gardin, and C. Sarrazin-Baudoux, ‘Fatigue crack growth versus plastic CTOD in the 304L stainless steel’, *Eng. Fract. Mech.*, vol. 214, no. April, pp. 487–503, 2019.

[32] A. M. Pereira, J. M. Ferreira, F. V. Antunes, and P. J. Bártolo, ‘Study on the fatigue strength of AA 6082-T6 adhesive lap joints’, *Int. J. Adhes. Adhes.*, vol. 29, no. 6, pp. 633–638, Sep. 2009.

[33] R. Branco *et al.*, ‘Low-Cycle Fatigue Behaviour of AISI 18Ni300 Maraging Steel Produced by Selective Laser Melting’, *Metals (Basel).*, vol. 8, no. 1, p. 32, 2018.

[34] D. Camas, P. Loureiro, P. Prates, and F. Antunes, ‘Numerical Determination of Fatigue Threshold from CTOD’, *Solid State Phenom.*, vol. 258, no. December, pp. 290–293, Dec. 2016.

[35] F. V. Antunes, P. Prates, D. Camas, and J. D. M. Costa, ‘Elastic correction of fatigue crack growth laws’, *Fatigue Fract. Eng. Mater. Struct.*, vol. 42, no. 5, 2019.

[36] J. Chakrabarty, *Applied Plasticity*, 2nd ed. 2010.

[37] P. Prates, ‘Inverse Methodologies for Identifying Constitutive Parameters of Metal Sheets’, PhD Thesis, Department of Mechanical Engineering, University of Coimbra, 2014.

[38] H. Tresca, ‘Memoir on the flow of solid bodies under strong pressure’, *Comptes Rendus l’Académie des Sci. Paris*, vol. 59, pp. 754–758, 1864.

[39] R. V. von Mises, ‘Mechanik der festen korper im plastic-deformablen zustand. Nachrichten vos der koniglichen gellesschaft des winssenschaften zu Gottingen’, *Math. klasse*, pp. 582–592, 1913.

[40] R. Hill, *The Mathematical Theory of Plasticity*. Oxford, UK, 1950.

[41] E. Voce, ‘The relationship between stress and strain for homogeneous deformation’, *J. Inst. Met.*, vol. 74, pp. 537–562, 1948.

[42] C. O. Frederick and P. Armstrong, *A Mathematical Representation of the Multiaxial Bauscinger Effect*, vol. 24. 2007.

[43] R. F. Simões, ‘Análise da Propagação de Fendas por Fadiga com Base no CTOD : Efeito dos Parâmetros Numéricos’, MSc Thesis, Department of Mechanical Engineering, University of Coimbra, 2017.

[44] M. Ashby, ‘CES EduPack’. 2018.

[45] L. S. Lasdon, A. D. Waren, A. Jain, and M. W. Ratner, ‘Design and testing of a generalized reduced gradient code for nonlinear optimization’, *Clevel. NTIS Natl. Tech. Inf. Serv. U. S. Dep. Commer.*, 1975.

[46] M. C. Oliveira, J. L. Alves, and L. F. Menezes, ‘Algorithms and strategies for treatment of large deformation frictional contact in the numerical simulation of deep drawing process’, *Arch. Comput. Methods Eng.*, vol. 15, no. 2, pp. 113–162, 2008.

[47] D. M. Neto, M. C. Oliveira, L. F. Menezes, and J. L. Alves, ‘Applying Nagata patches to smooth discretized surfaces used in 3D frictional contact problems’, *Comput. Methods Appl. Mech. Eng.*, vol. 271, pp. 296–320, 2014.

[48] L. F. Menezes and C. Teodosiu, ‘Three-dimensional numerical simulation of the deep-drawing process using solid finite elements’, *J. Mater. Process. Technol.*, vol. 97, no. 1–3, pp. 100–106, 2000.

[49] R. Heleno, ‘Desenvolvimento de uma plataforma interactiva para a utilização do DD3IMP’, MSc Thesis, Department of Mechanical Engineering, University of Coimbra, 2012.

[50] B. Marques, ‘Análise da propagação de fendas por fadiga utilizando o CTOD’, MSc Thesis, Department of Mechanical Engineering, University of Coimbra, 2019.

[51] J. M. Vasco-Olmo, F. A. Díaz, F. V. Antunes, and M. N. James, ‘Characterisation of fatigue crack growth using digital image correlation measurements of plastic CTOD’, *Theor. Appl. Fract. Mech.*, vol. 101, pp. 332–341, Jun. 2019.

[52] D. Tortorelli and P. Michaleris, ‘Original Articles Design sensitivity analysis: Overview and review’, *Inverse Probl. Sci. Eng.*, vol. 1, no. 1, pp. 71–105, 1994.

[53] K.-H. Schwalbe, ‘Comparison of several fatigue crack propagation laws with experimental results’, *Eng. Fract. Mech.*, vol. 6, no. 2, pp. 325–341, Sep. 1974.

[54] D. A. Jablonski, J. V. Carisella, and R. M. Pelloux, ‘Fatigue crack propagation at elevated temperatures in solid solution strengthened superalloys’, *Metall. Trans. A*, vol. 8, no. 12, pp. 1893–1900, 1977.

[55] S. Chand and S. B. L. Garg, ‘Crack propagation under constant amplitude loading’, *Eng. Fract. Mech.*, vol. 21, no. 1, pp. 1–30, Jan. 1985.

[56] R. P. Skelton, T. Vilhelmsen, and G. A. Webster, ‘Energy criteria and cumulative damage during fatigue crack growth’, *Int. J. Fatigue*, vol. 20, no. 9, pp. 641–649, Oct. 1998.

[57] M. Clavel and A. Pineau, ‘Fatigue behaviour of two nickel-base alloys I: Experimental results on low cycle fatigue, fatigue crack propagation and substructures’, *Mater. Sci. Eng.*, vol. 55, no. 2, pp. 157–171, Sep. 1982.

[58] H. W. Liu, ‘Fatigue crack growth by crack tip cyclie plastic deformation: the unzipping model’, *Int. J. Fract.*, vol. 39, no. 1–3, pp. 63–77, 1989.

[59] H. W. Liu and D. Liu, ‘A quantitative analysis of structure sensitive fatigue crack growth in steels’, *Scr. Metall.*, vol. 18, no. 1, pp. 7–12, Jan. 1984.

ANNEX A - PAPERS

This section presents the front pages of the papers in development “Effect of Young´s modulus on Fatigue Crack Growth” and “Effect of yield stress on Fatigue Crack Growth”. The last paper will be submitted for publication to the Journal of Fracture and Structural Integrity.

It also presents a paper published in Structural Integrity Procedia.

Effect of Young's modulus on Fatigue Crack Growth

MF Borges[a], FV Antunes[1a], PA Prates[a], R Branco[a] T Vojtek[b]

[a] CEEMPRE, Department of Mechanical Engineering, University of Coimbra, Portugal

[b] Central European Institute of Technology (CEITEC), Brno University of Technology, Czech Republic

Abstract

The study of the effect of material parameters on fatigue crack growth (FCG) rarely have been addressed in the literature. The objective is to study the effect of Young modulus on FCG using a numerical approach. A methodology based on the plastic CTOD was used to develop this parametric study. FCG rate was found to increase linearly with 1/E, which is according most of the models proposed in the literature. The decrease of rigidity increases the elastic deformation, as expected. There is a link between the elastic and the plastic deformation which explains the increase of plastic CTOD and therefore of FCG rate.

Keywords: Young's modulus; plastic CTOD; Fatigue Crack Growth Rate

[1] Corresponding author: e-mail: fernando.ventura@dem.uc.pt; Fax: 00351 239 790701

Effect of yield stress on fatigue crack growth

MF Borges, FV Antunes, P Prates, R Branco, MC Oliveira
CEEMPRE, Department of Mechanical Engineering, University of Coimbra

micaelfriasborges@outlook.pt
fernando.ventura@dem.uc.pt, http://orcid.org/0000-0002-0336-4729
pedro.prates@dem.uc.pt,
ricardo.branco@dem.uc.pt,
marta.oliveira@dem.uc.pt,

ABSTRACT. Fatigue crack growth (FCG) depends on loading, geometry and also material properties. Since FCG is supposedly linked to crack tip plastic deformation, material's yield stress, Y_0, is an important parameter. The main objective here is to develop a parametric study focused on the effect of Y_0 on FCG. The study is based on the plastic CTOD, δ_p, determined numerically using the finite element method. The increase of Y_0 was found to decrease δ_p, and therefore FCG rate. The variation is non-linear, being more important for lower values of Y_0. The effect of Y_0 was found to be much more relevant for the 7050 aluminium alloy than for the 304L stainless steel, which indicated a major influence of isotropic saturation stress. With the inclusion of crack closure, the reduction of δ_p is kept, but there is a substantial reduction of δ_p and therefore of FCG rate.

KEYWORDS. Fatigue Crack Growth; plastic CTOD; yield stress; crack closure

OPEN ACCESS

Citation: AuthorA, N., AuthorB, N., AuthorC, N., AuthorD, N., Title title title, Frattura ed Integrità Strutturale, xx (2018) ww-zz.

Received: xx.yy.zzzz
Accepted: xx.yy.zzzz
Published: xx.yy.zzzz

Available online at www.sciencedirect.com

ScienceDirect

Structural Integrity Procedia 00 (2019) 000–000

Structural Integrity Procedia

www.elsevier.com/locate/procedia

9th International Conference on Materials Structure and Micromechanics of Fracture

Crack tip mechanisms: a numerical analysis

FV Antunes[a], MF Borges[a], B Marques[a], P Prates[a], R Branco[a]*

[a] CEEMPRE, University of Coimbra, Rua Luís Reis Santos, 3030-788 Coimbra, Portugal

Abstract

Fatigue crack propagation is usually studied using da/dN-ΔK curves obtained experimentally. However, the use of ΔK does not provide any information into the mechanics which occur at the crack tip and are effectively responsible for fatigue crack growth. The objective here is to study crack tip phenomena using the CTOD. The aspects studied are the crack closure level, the elastic regime of ΔK and the crack tip plastic deformation, which was related with fatigue crack propagation. The elastic load range, ΔK_{el}, was found to increase linearly with material's yield stress. Well defined relations were found between the elastic and the plastic deformations, which greatly depend on material. The fatigue crack growth rate, obtained experimentally, was plotted versus plastic CTOD range, δ_p, for the different materials. Finally, the CTOD versus load curves were used to predict fatigue threshold and to study material hardening after crack propagation.

Peer-review under responsibility of the scientific committee of the IC MSMF organizers.

Keywords: Fatigue crack propagation; CTOD; crack closure; fatigue threshold.

ANNEX B – TABLE

Table B.1. Fatigue crack growth models which include fatigue threshold.

Reference	Model	Comments
Erdogan and Ratwani [4]	$\frac{da}{dN}=\frac{C(1+\beta)^m(\Delta K-\Delta K_{th})^m}{K_c-(1+\beta)\Delta K}$	$\beta=\frac{K_{max}+K_{min}}{K_{max}-K_{min}}$
Hartman and Schijve [5]	$\frac{da}{dN}=\frac{D'(\Delta K-\Delta K_{th})^\alpha}{(1-R)K_c-\Delta K}$	K_C – Fracture toughness D, α - material constants
Pelloux [25]	$\frac{da}{dN}=\frac{2\Delta K^2}{\pi E Y_0}$	
Nicholls [27]	$\frac{da}{dN}=\frac{\Delta K^4}{4EY_0K_c^2}$	
Schwalbe [53]	$\frac{da}{dN}=\beta\frac{\Delta K^2}{4\pi(1+n)Y_0^2}(\frac{2Y_0}{\varepsilon_f E})^{1+n}$	ε_f – failure strain n – hardening exponent
Jablonski [54]	$\frac{da}{dN}=\frac{0.0338(1-\nu^2)}{\varepsilon_f EY_0}\Delta K^2$	n=10
Chand and Garg [55]	$\frac{da}{dN}=\frac{0.15\Delta K_{eff}^2 Y_0}{nEK_{Ic}^2(1+R)^{3.8}}$	K_{Ic} – fracture toughness
Skelton *et al.* [56]	$\frac{da}{dN}=\frac{\Delta K^2(1-\nu)}{2\pi E W_c}$	W_c – critical value of density of cumulative energy
Clavel and Pineau [57]	$\frac{da}{dN}=\beta\frac{\Delta K^2}{EY_0}$	β=0.25 Clavel and Pineau $\beta=0.02(1-\nu^2)$ Liu [58]
Liu and Liu [59]	$\frac{da}{dN}=\frac{0.036}{EY_0}(\Delta K-\Delta K_{th})^2$	